Morphodynamic impacts of large-scale engineering projects in the Yangtze River delta

Luan, Hualong; Ding, P; Wang, Zhengbing ; Yang, S.L.; Lu, Jin You

DOI
10.1016/j.coastaleng.2018.08.013

Publication date
2018

Document Version
Accepted author manuscript

Published in
Coastal Engineering

Citation (APA)
Luan, H., Ding, P., Wang, Z., Yang, S. L., & Lu, J. Y. (2018). Morphodynamic impacts of large-scale engineering projects in the Yangtze River delta. *Coastal Engineering*, *141*, 1-11. https://doi.org/10.1016/j.coastaleng.2018.08.013

Morphodynamic impacts of large-scale engineering projects in the Yangtze River delta

Hua Long Luan [a], Ping Xing Ding [a, *], Zheng Bing Wang [a, b, c], Shi Lun Yang [a], Jin You Lu[a]

[a] State Key Laboratory of Estuarine and Coastal Research, East China Normal University, Shanghai 200062, China

[b] Faculty of Civil Engineering and Geosciences, Delft University of Technology, P.O. Box 5048, 2600 GA Delft, The Netherlands

[c] Deltares, P.O. Box 177, 2600 MH Delft, The Netherlands

*Corresponding author.

Tel: +86 021-62232897

Fax: +86 021-62233468

E-mail address: pxding@sklec.ecnu.edu.cn (Prof. P.X. Ding)

Highlights

- ✓ The seaward part of the mouth bar area converted from accretion to overall erosion along with river sediment reduction since 1997.
- ✓ Morphodynamics of the mouth bar area since 1997 show distinct spatiotemporal variations.
- ✓ The training walls along the North Passage significantly modified the hydrodynamics in the mouth bar area.
- ✓ The downstream half of the north dike contributed to the accretion at the East Hengsha Shoal and erosion at seaward end of the North and South Passage.

Abstract

Impacts of local human interventions on morphodynamics of large river deltas are insufficiently understood, especially superimposed upon delta erosion due to diminishing sediment supplies. The densely populated Yangtze Estuary in China is increasingly influenced by large-scale estuarine engineering projects in the recent two decades and thereby provides a useful example to address this issue. This work investigates the morphological impacts of the Deepwater Navigation Channel Project (DNCP) including dikes and groynes implemented in 1997-2010 on the mouth bar area of the Yangtze Estuary through data analysis and process-based modeling approach (Delft3D). The seaward portion of the mouth bar area, defined as the study area for calculation of sediment volume change, converted from net accretion to net erosion during 1997-2013 primarily due to river sediment reduction. However, the East Hengsha Shoal (EHS) showed abnormal accretion in the same period. The accretion-erosion conversion occurred around the year 2004 is largely contributed by two erosion zones at the northern and southern subaqueous delta, respectively. Hydrodynamic simulations indicate that the training walls result in weaker tidal flow and longer slack period at the EHS and stronger tidal flow at the southern erosion zone. Subsequently, morphological modeling demonstrates that the training walls enhance accretion at the EHS, which is mainly attributed to the downstream half of the north dike. This can be verified by the consistent period (2002-2004) of the dike extension to the present location and accretion peak of the EHS. Morphological modeling also indicates that the downstream half of the north dike enhanced erosion at the southern erosion zone, which can partly explain the gradual increase in the erosion volume of both erosion zones after 2004. Under large-scale estuarine engineering projects, the Yangtze subaqueous delta is accelerating to approach morphodynamic equilibrium. The timescale to the erosion limit and sustainable estuarine management merit further systematic research.

Keywords: Morphodynamics; River sediment reduction; Estuarine engineering projects; Mouth bar area; Yangtze Estuary

1. Introduction

Modern deltas across the globe, originated since the maximum Holocene transgression (Stanley and Warne, 1994), are actively propagating systems as redundant fluvial sediment accumulated hereon after part of the amount being taken away by marine currents (Coleman and Wright, 1975; Syvitski and Saito, 2007). Anthropogenic activities in drainage basins strongly modified such propagation processes by increasing sediment productions over the past millennia and decreasing sediment loads in the past century (Milliman et al., 1987; Hori et al., 2001; Syvitski et al., 2005). Though the definition of the Anthropocene in the geological sense is controversial (Syvitski and Kettner, 2011; Renaud et al., 2013), there is no doubt that morphodynamics of world's deltas are altering from natural evolution driven to anthropogenic impact driven (Syvitski and Saito, 2007). Engineering controls within deltaic plains, particularly in the recent decades, are likely to accelerate the alteration process superimposed upon the effect of low sediment supply due to upstream dam construction and improved soil conservation (Vörösmarty et al., 2003; Walling, 2006). Therefore, it is urgently needed to strengthen our understanding on the morphodynamics of these dynamic and vulnerable environments, regarding that deltas are home to more than half a billion people and thousands of plant and animal species (Giosan et al., 2014), and thereby hold high ecological and socio-economic value (Day et al., 1989).

The fluvial sediment reduction compounded with rising seas has resulted in delta erosion and flooding around the world (Ericson et al., 2006; Syvitski et al., 2009). The close link between human-induced decrease of sediment loads and delta erosion is identified by numerous case studies on large deltas, including the Nile (Stanley, 1996), Mississippi (Blum and Roberts, 2009), Ebro (Sanchez-Arcilla et al., 1998), Mekong (Anthony et al., 2015), and Yellow (Chu et al., 2006; Wang et al., 2007). Most densely populated deltas were further interfered by vicinal human interventions. The Mississippi River Delta, for instance, is suffering from rapid subsidence and land loss caused by intensive hydrocarbon extraction (Morton et al., 2005). Flow path control of distributary channels also produced remarkable impacts on delta evolution as occurred in Colorado, Po and Yellow deltas (Syvitski and Saito, 2007). Other local interventions include training wall construction, dredging, reclamation, etc. (Blott et al., 2006; Wu et al., 2016). Rapid urbanization and resource utilization within deltaic areas are likely to aggravate the risk and sustainability of deltas (Syvitski, 2008).

The Yangtze River delta in China provides a useful example to examine deltaic morphodynamics under human interventions because this large-scale and densely populated delta is heavily impacted by human activities from both the upstream reach and deltaic region (Fig. 1a) (De Vriend et al., 2011). Many estuarine engineering projects have been conducted in the recent 2 decades for navigation, flood control, freshwater consumption and wetland management purposes (Tian et al., 2015; Luan et al., 2016). Present study concentrates on the mouth bar area and adjacent part of the subaqueous delta spanning from the East Hengsha Shoal (EHS) and Jiuduansha Shoal (JS) to the isobath of nearly 30 m (Fig. 1b), which have been significantly interfered by estuarine engineering projects since 1997 (Luan et al., 2016).

Under decreasing river sediment supply after the constructions of more than 50,000 dams throughout the watershed (Yang et al., 2011), multiple evidences for overall delta erosion have been identified in terms of bed level changes (Yang et al., 2011), grain size variations (Luo et al., 2017), sediment transport capacity of coastal currents (Deng et al., 2017) and isotopic tracing (Wang et al., 2017). Dai et al. (2014) reported that the Yangtze subaqueous delta rebounded from slight erosion to high accumulation with much higher accumulation amount than river sediment supply after the operation of the Three Gorge Dam (TGD) in 2003, whereas the sources of the excess sediment and relevant processes for sediment re-distribution remained unknown. Zhu et al. (2016) demonstrated that the recent erosion of the subaqueous delta can be related to the training walls along the North Passage which significantly modified the estuarine hydrodynamics as suggested by a model-based study. Luan et al. (2016) found that the northern part of the mouth bar area, particularly the EHS, converted from net erosion in 1986-1997 to net accretion in 1997-2010. The mouth bar area in the latter period showed slightly net accretion though simultaneous erosion in its southern part was observed. However, Luan et al. (2016) only provided the morphological difference of the mouth bar area before and after the constructions of training walls. Neither the evolution processes within the period (1997-2010) nor the physical mechanisms responsible for the enhanced accretion at the EHS were investigated. Furthermore, the separated influences of estuarine human interventions and river sediment reduction on morphological changes are still less understood. Therefore, this study combines bathymetric data analysis and process-based modeling approach (Delft3D) to examine the morphological evolution and mechanisms of the mouth bar area under large-scale estuarine engineering projects since 1997. The results should be valuable for sustainable management of the Yangtze Estuary and other densely populated river deltas in the world.

2. Study area

The Yangtze River, ranking the largest and longest in Asia (Milliman and Farnsworth, 2013), reaches its end near Shanghai City and enters the inner shelf of the East China Sea (Fig. 1a). Abundant river sediment supply contributed to rapid delta progradation with approximately 50 km per millennium since the mid-Holocene (Hori et al., 2001). Currently, the Yangtze subaqueous delta covers an area of over 10,000 km^2 spanning from the crest of the mouth bar to the paleo-incised valley (30-50 m) (Chen et al., 1985). The seabed at the mouth bar area is dominated by fine cohesive mud which can be frequently resuspended by tidal currents (Liu et al., 2010; Luo et al., 2012). This area behaves as both the estuarine turbidity maximum and depocenter of the delta (Chen et al., 1985; Dai et al., 2014). Mean tidal range and wave height at the mouth is 2.67 m and 0.9 m, respectively (Yun, 2004). Meanwhile, the delta receives huge amount of river inputs from the upstream river, i.e. 896 km^3/yr of runoff and 390 Mt/yr of suspended sediment load in 1950-2010 (CWRC, 2011). Under combined large river flow, meso-tidal and minor wave forcing, the Yangtze River delta is defined as a mixed river- and tidal-dominant mud delta and featured by a funnel-shaped topography with wide distributary channels and accreting intertidal flats (Fig. 1b).

No significant variation trend was observed for the annual water runoff in the past half century, while the annual sediment load remained at a high level in the 1950-1960s and decreased continuously after the 1980s (Fig. 2). The decreasing trend was accelerated since the late 1990s and gradually vanished after the closure of the TGD in 2003 (Fig. 2). The sediment load retained at a relatively low level in the post-TGD decade (145 Mt/yr) which is only about 30% of that in 1950-1968 (Yang et al., 2015). Notably, the sediment load was as low as 85 Mt/yr and 72 Mt/yr in the extreme drought year 2006 and 2011, respectively (Fig.

2).

Under the condition of low sediment supply in the recent 2 decades, many engineering projects have been constructed within the estuarine area. One of the largest in the study area is the Deep Navigation Channel Project (DNCP) along the North Passage (Fig. 1b) which was aimed at improving the navigational capacity. The DNCP was implemented through three phases from 1998 to 2010 including constructions of training walls and intensive dredging. The upstream and downstream parts of the dikes and groynes were constructed in Phase I (1998.01-2002.06) and Phase II (2002.05-2004.12), respectively, resulting in 100.7 km as the total length of the twin dikes and 19 perpendicular groynes (Fig. 1c). The bathymetry within the North Passage responded rapidly to the constructions of training walls through severe deposition in the dike-sheltered areas and siltation in the navigational channel (Liu et al., 2011; Dai et al., 2013). Phase III (2006.09-2010.03) of the project mainly includes the construction of submerged dikes in the south side, groyne extensions and dredging (Fig. 1c). As a consequence, the deep navigation channel between the north and south dike was deepened from 6.5 m before the project in 1998 to 8.5 m in 2001, 10 m in 2005 and 12.5 m in 2011. Thus, the mouth bar in the North Passage was broken through after a plenty of dredging efforts. Other engineering projects within the mouth bar area include the land reclamation at EHS and East Nanhui Mudflat, which also heavily impacted the morphological evolution of the Yangtze Estuary (Wei et al., 2015).

3. Method

3.1 Data collection and processing

To assess the morphological processes during estuarine engineering projects, we collected navigational charts and bathymetric maps based on observations in various years (1997, 2002, 2004, 2007, 2010 and 2013) which captured each phase of the DNCP (Tab. S1). An echo sounder and a global positioning system (Trimble Navigation Limited, California, USA) were used for depth measurements and position recordings, respectively, with vertical and horizontal errors of 0.1 m and 1 m. In line with the analyzing procedure by Luan et al. (2016), the depth points digitized from navigational charts are combined with bathymetric maps to cover the whole mouth bar area and adjacent part of subaqueous delta (Fig. S1). The scales of the maps range from 1:50,000 to 1:130,000 (Tab. S1), and the averaged data density ranges from 1.1 to 11.5 samples/km^2 which is sufficiently high for calculation of morphological evolution with acceptable accuracy (Dai et al., 2014; Luo et al., 2017). Depth points of each year, referenced to the theoretical lowest-tide datum at Wusong, are interpolated into a 50×50 m grid by the Kriging interpolation technique in the Surfer mapping software package. Consequently, a digital elevation model (DEM) is generated for each year of bathymetric data (Fig. 3a1-f1). The erosion/deposition patterns are obtained by subtracting a later DEM from an earlier one (Fig. 3a2-e2). We assume that the dominant cause for water depth variation is bed sediment erosion and deposition (Yang et al., 2011; Dai et al., 2013, 2014). Inspired by Yang et al. (2011) and Zhu et al. (2016), a rectangle domain covering seaward of the mouth bar area and adjacent part of the subaqueous delta is chosen for erosion/deposition calculations. The North Passage and the dredged navigation channel are excluded from the study area as this study aims at exploring training-wall-induced bathymetric changes of the mouth bar area beyond the North Passage (Fig. 1b). In order to investigate the spatial differences of the morphological changes, the study area are firstly divided into a northern part and a southern part by an eastward extending line of the northern dike. The 10m-isobath in 1997 is used to further separate the two parts into four sub-areas in total, i.e. Areas N1, N2, S1 and S2 (Fig. 4a). The erosion/deposition area percentages, yearly sediment volume changes and net changes of the whole study area and four sub-areas are calculated based on the bed-level changes, grid resolution, domain areas and year spans (Luan et al., 2016)

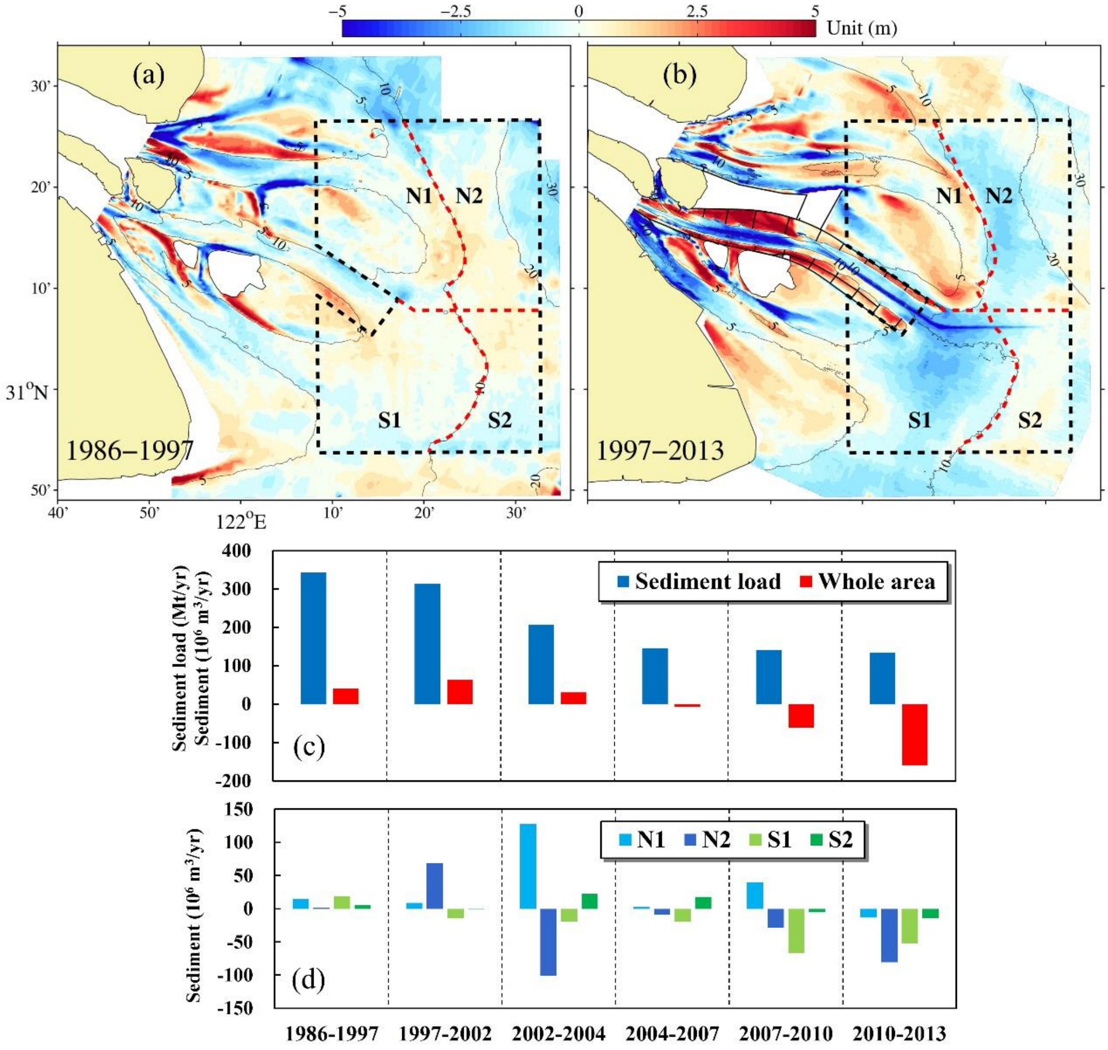

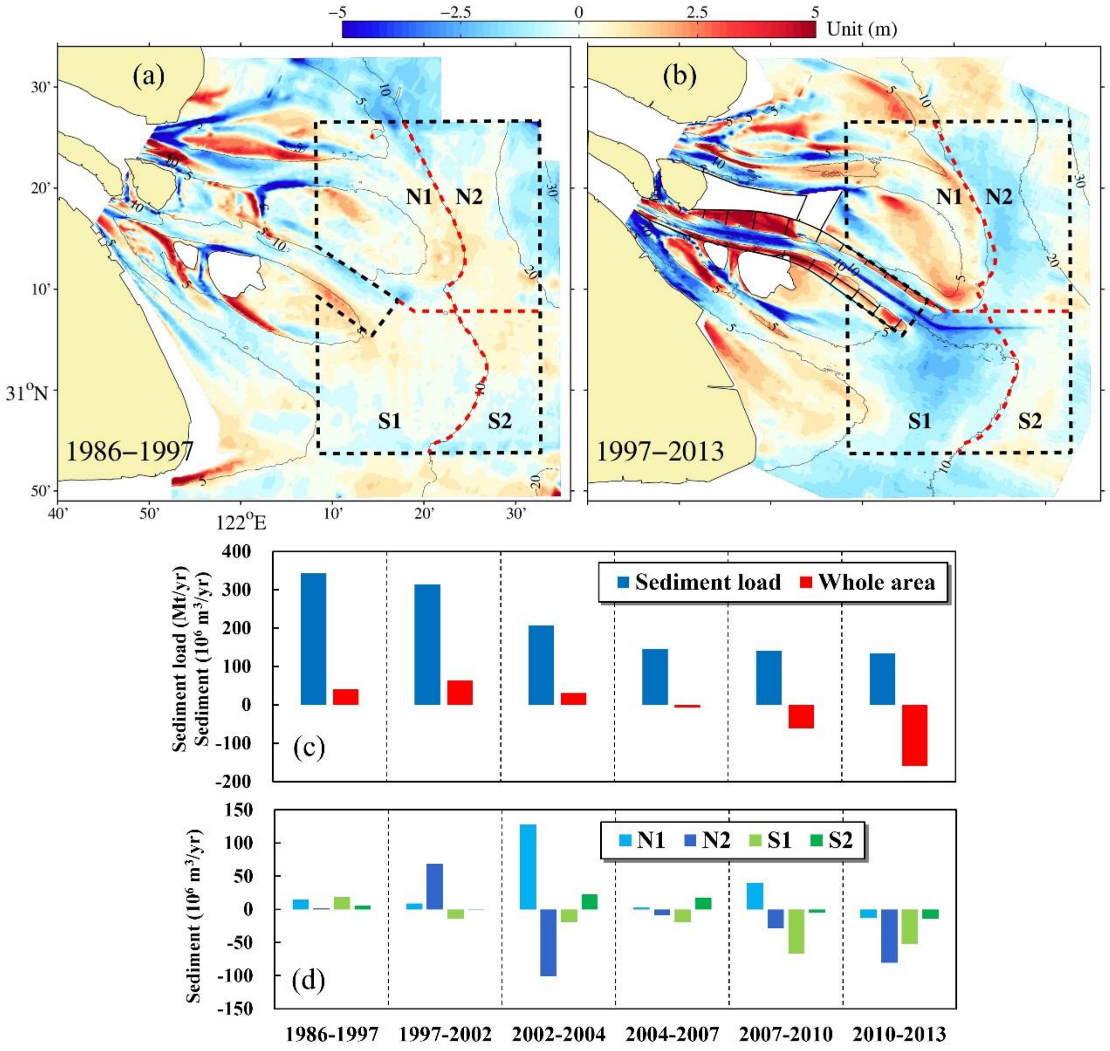

(Fig. 4c, d; Tab. S2, S3). Three typical sections in the study area (Fig. 5) are extracted from the DEM to describe the amplitudes of bed-level changes.

3.2 Process-based morphological modeling

The process-based Delft3D model system is applied to examine the impacts of training walls on hydrodynamics and morphological changes. The model solves shallow water equations under hydrostatic pressure assumption in a horizontal curvilinear grid and is fully integrated with hydrodynamic, sediment transport and morphological updating modules (Lesser et al., 2004). Medium- to long-term morphodynamic modeling can be implemented through linearly accelerating bed-level change each hydrodynamic time step with a carefully selected morphological factor (MF) (Roelvink, 2006). Thus, the model online couples flow and morphology and produces bathymetric change in an up-scaled period. Numerous case studies have demonstrated high capacity of the Delft3D model system on reproducing detailed flow features, sediment dynamics and morphological evolution of coastal and estuarine systems (van der Wegen et al., 2011; Dissanayake et al., 2012; van Maren et al., 2015; Su et al., 2016; Luan et al., 2017).

The morphological model of the Yangtze Estuary applied in this study considers tidal forcing, river discharge, wind wave, sediment transport and online bed-level change. Variations in river inputs and multiple sediment fractions (cohesive and noon-cohesive) are included in the model due to strong river seasonality and highly graded bed sediment within the estuarine area. Promising hindcasting of the decadal morphodynamic evolution of the Yangtze Estuary were carried out for three historical periods involving distinct morphological processes, a rapid accretion period (1958-1978), an erosional period (1986-1997) and a recent period with slight accretion (2002-2010). Details of the model setup and hindcast results were described by Luan et al. (2017). Hindcast case of the recent period which corresponds to the constructing period of the DNCP shows best model performance and thereby provides a nice reference case for investigating impacts of training walls on hydrodynamics and morphological evolution. One numerical experiment is firstly conducted which excludes all the dikes and groynes along the North Passage from the reference case to explore the overall impacts of the training walls. The northern and southern dikes were extended to the present location after the Phase II of the DNCP and induced severe siltation in the middle of the dredged channel (Liu et al., 2011). Dikes implemented in Phase II are close to the EHS and the observed erosion zones at the subaqueous delta (Luan et al., 2016; Zhu et al., 2016). Therefore, two further numerical experiments are conducted which exclude the downstream half of the northern and southern structures from the reference case, respectively. The modeled hydrodynamics, sediment transport processes and subsequent bed-level changes in the above three experiments are compared with the reference case to provide physical explanations of the observed evolution under large-scale estuarine engineering projects.

4. Results

4.1 Morphological changes during 1997-2013

The erosion/deposition patterns during 1997-2013 show distinct spatial variations, reflected by accretion at the EHS and erosion at the seaward end of the North and South Passage

(

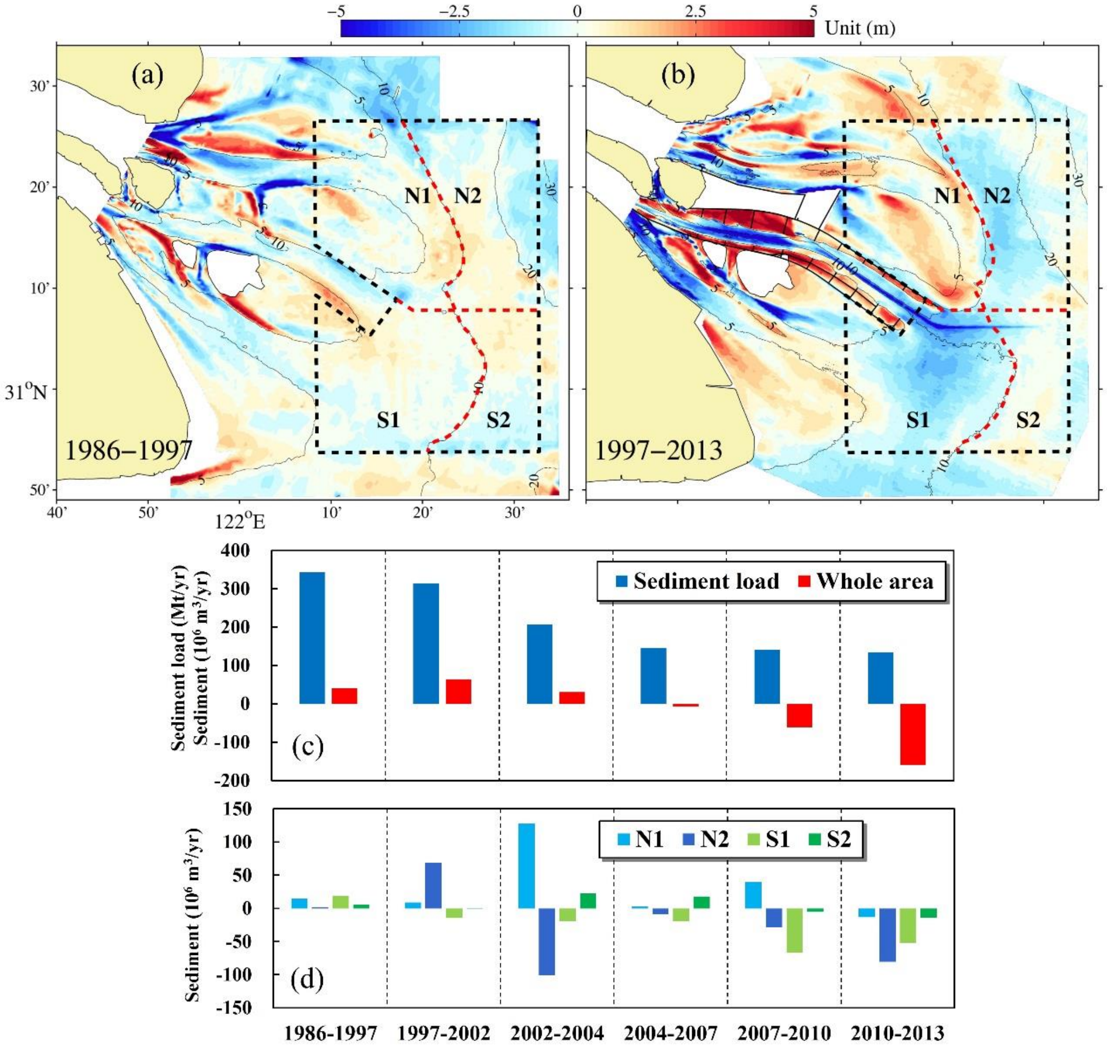

Fig. 4b). For the comparison purpose, the pattern in 1986-1997 is also presented

(

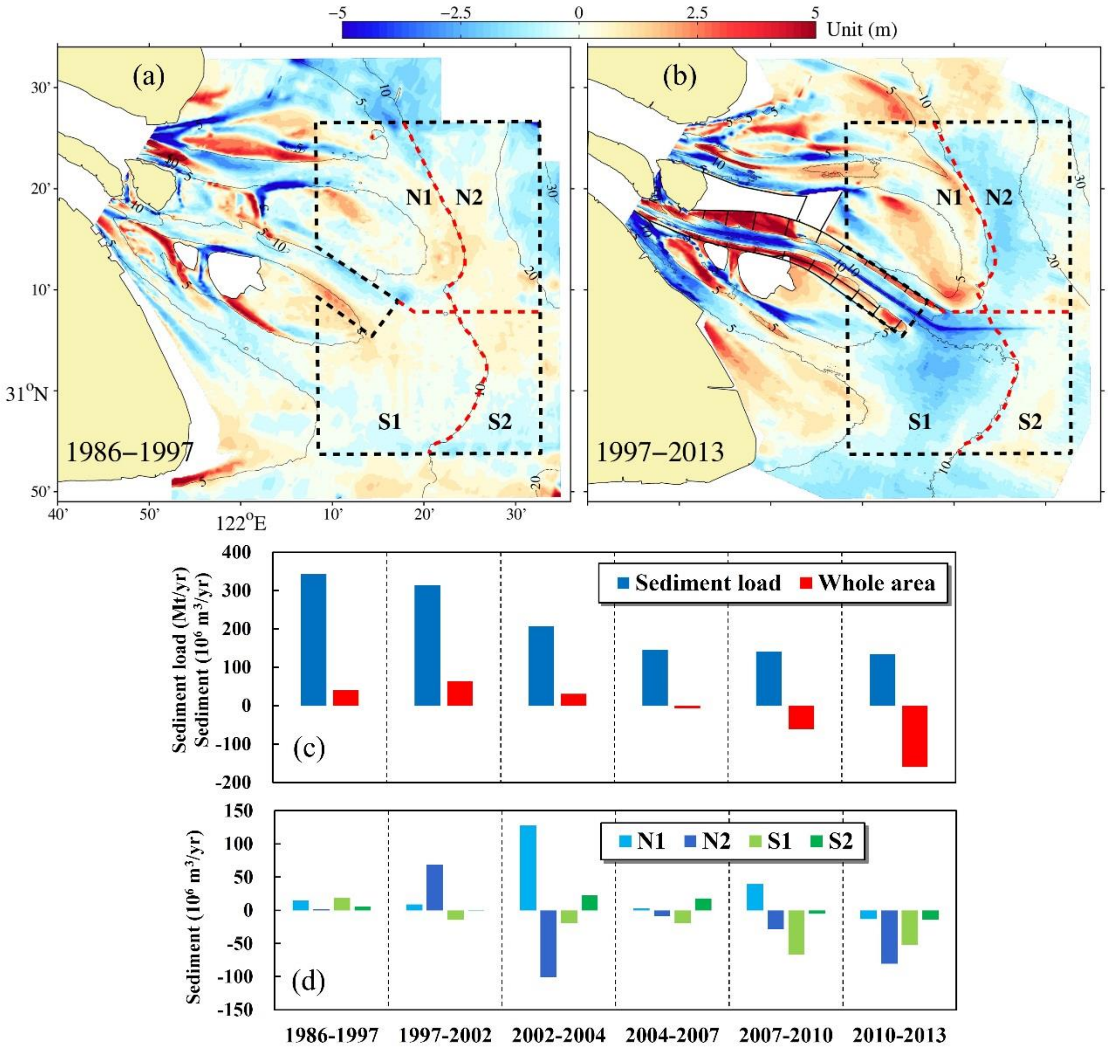

Fig. 4a). The latter area involved strong deposition in 1986-1997 as higher river sediment discharge fed the delta. On the contrary, accretion at the EHS increased from 1986-1997 to 1997-2013 under decreased sediment supply. In addition to similar descriptions by Zhu et al. (2016), the morphological evolution processes in shorter intervals (2-5 years) within the period (1997-2013) are presented (Fig. 3a2-e2). The patterns indicate that continuous erosion occurred at the seaward end of North and South Passage since 1997, while accretion at the EHS peaked in 2002-2004 and decreased after 2004 (Fig. 3b2). The deep part (>10 m) of the northern subaqueous delta converted from deposition to erosion around the year 2002 and showed continuous erosion in 2002-2013. The deep part (>10 m) of the

southern subaqueous delta experienced episodic deposition and erosion in the study period. In 2010-2013, the mouth bar area and adjacent part of the subaqueous delta were dominated by overall erosion (Fig. 3e2).

Sediment volume changes provide quantitative assessment of morphological evolution. As shown in the Fig. 4c, a coherent conversion from net accretion to erosion of the whole study area occurred around the year 2004 along with the decreasing sediment supply. The net accretion volume increased from 40.6 Mm^3/yr in 1986-1997 to 63.6 Mm^3/yr in 1997-2002, possibly due to much longer time span of the earlier period and thereby bed sediment compaction during

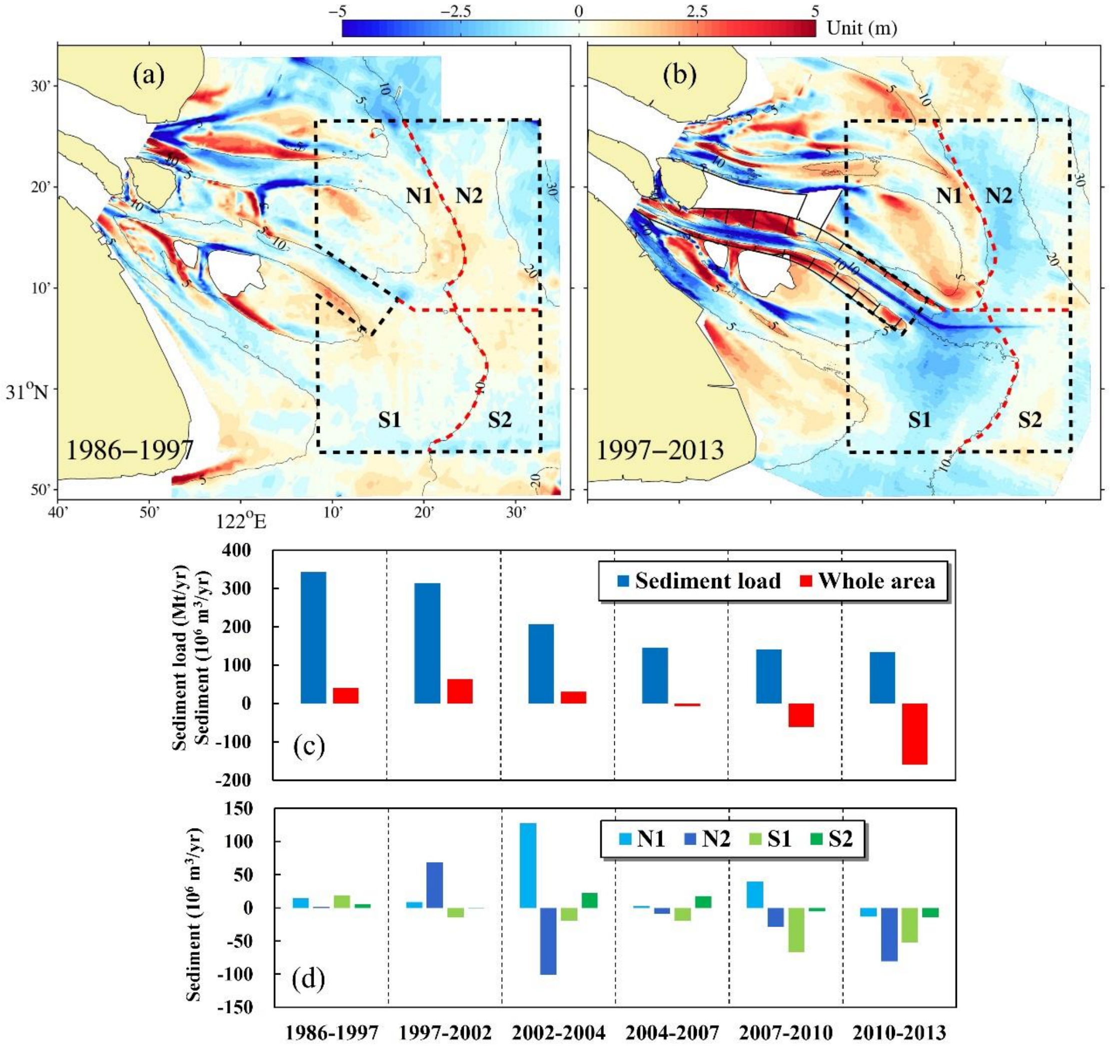

the same period. The sediment discharge decreased from 251 Mm^3/yr in 1997-2002 to 117 Mm^3/yr in 2004-2007, and the decreasing rate slowed down significantly in the later two periods, i.e. 113 Mm^3/yr in 2007-2010 and 107 Mm^3/yr in 2010-2013 (Tab. S2). However, the net erosion amount showed almost linear increase from −7.0 Mm^3 yr^{-1} in 2004-2007 to −159.6 Mm^3 yr^{-1} in the latest period, and the net erosion rate reached as high as −71.8 mm yr^{-1} in the latest period (Fig. 4c; Tab. S2). The proportion of accretion area in the whole area decreased monotonously during the period 1986-2013 (Tab. S2), and the accretion area became less than

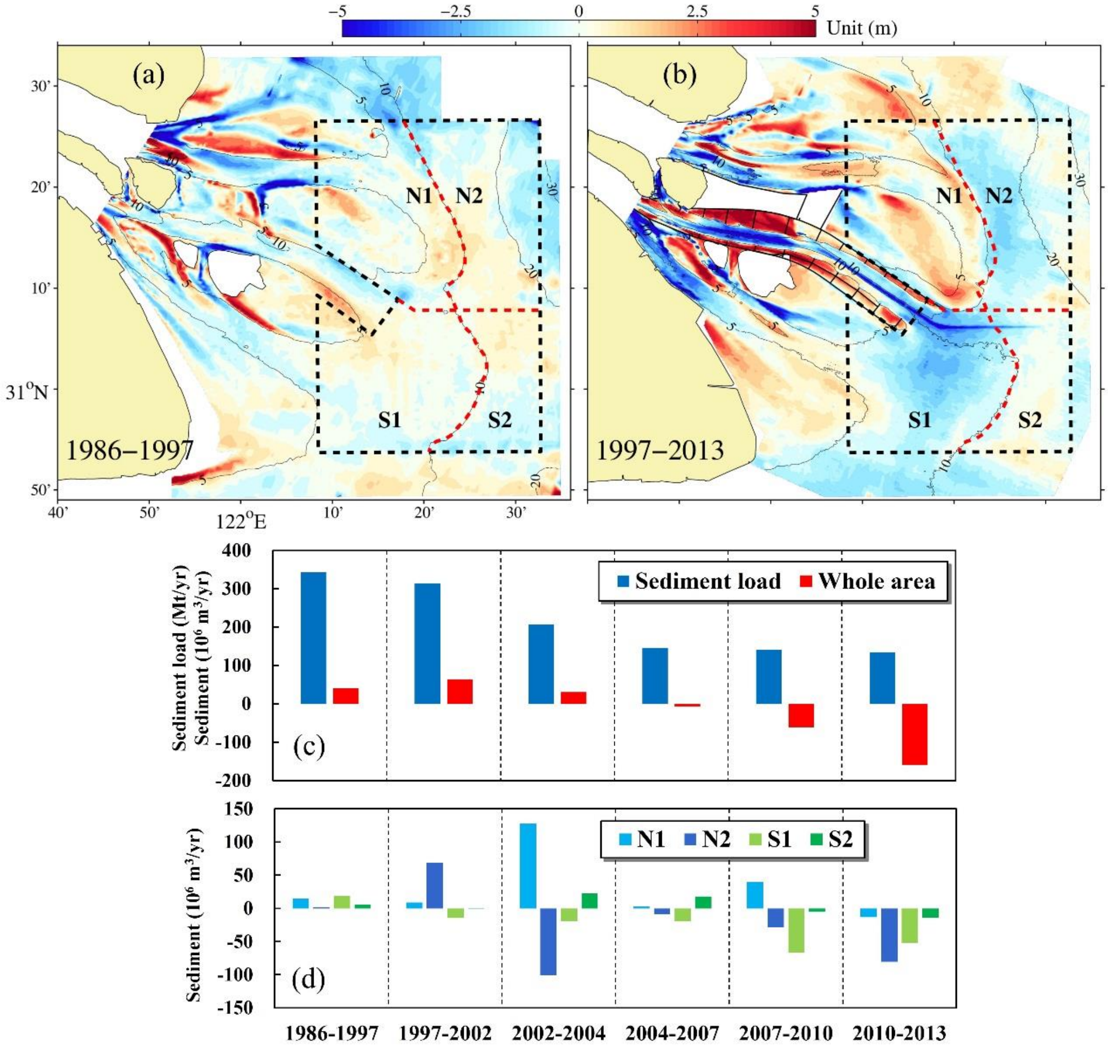

the erosion area after 2004 which was consistent with the trend of sediment volume changes.

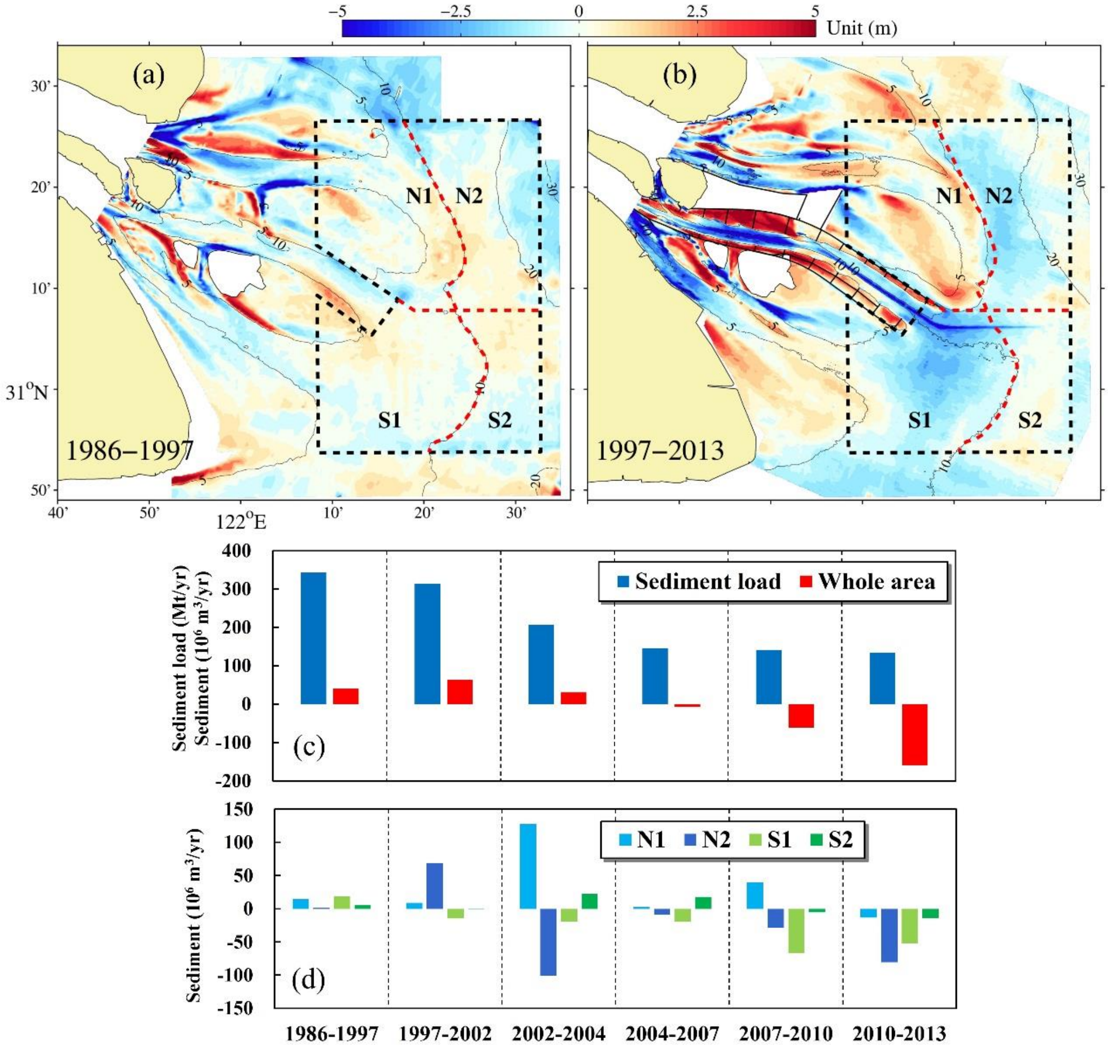

Four sub-areas feature distinct morphological behaviors compared with the whole area in terms of sediment volume variations (Fig. 4d). All the sub-areas were under net accretion in 1986-1997 with relatively low net accretion amount which was subject to bed sediment compaction. In the five periods from 1997 to 2013, the sub-areas involved alternate net accretion or erosion as described below. The Area N1, mainly covering the EHS, experienced net accretion in the first four periods and net erosion in the latest one. The net accretion volume and rate peaked in 2002-2004 (127.7

Mm^3 yr^{-1} or 195.2 mm yr^{-1}) (Tab. S3), and the values in other periods were relatively low. This was also indicated by hypsometry curves of the northern part in which the shallow water area (2~6.5 m) decreased abruptly from 2002 to 2004, suggesting rapid accretion (Fig. S2a). The Area N2, representing the northern erosion zone, involved high accretion amount in 1997-2002 (68.6 Mm^3 yr^{-1}) and altered into continuous erosion in the following four periods. The strongest erosion was observed in 2002-2004 (−100.7 Mm^3 yr^{-1}) corresponding to the accretion peak of the Area N1. Afterwards, the net erosion amount dropped sharply to a low value in 2004-2007 (−8.6 Mm^3 yr^{-1}) and increased gradually to −80.6 Mm^3 yr^{-1} in 2010-2013. Accordingly, the area deeper than 10 m increased remarkably twice, i.e. from 2002 to 2004 and from 2010 to 2013 (Fig. S2a). The Area S1, representing the southern erosion zone, underwent increasing erosion in all the five periods except slightly decreased erosion rate in 2010-2013. Erosion in the southern part primarily occurred in the depth range of 5-10 m which corresponded to the Area S1 (Fig. S2b). The total net erosion volume of the Area N2 was −50.5 Mm^3 yr^{-1} from 2002 to 2013, while the value of the Area S1 was −32.7 Mm^3 yr^{-1} from 1997 to 2013. The Area S2, representing adjacent part of the subaqueous delta, converted from net accretion to net erosion around the year 2007. Both the accretion and erosion amount were small suggesting slow morphological changes in this area. Notably, all the sub-areas showed net erosion in 2010-2013, indicating that the mouth bar area had undergone overall erosion under a low level of river sediment supply for a sufficiently long time.

Variations of the typical cross-sections provide information on the erosion/deposition thickness (Fig. 5). An erosion band along the north dike formed with deepening of 2 m in

1997-2013 (Fig. 5a, d). Both the accretion thickness at the central EHS and the erosion thickness at the northern erosion zone were nearly 2 m (Fig. 5a, d). The seabed at southeast end of the EHS had risen up to about 3.5 m in 1997-2013 (Fig. 5c, d). Meanwhile, the maximum erosion thickness of the southern erosion zone was about 2.5 m (Fig. 5b, d). The dredging activities caused continuous deepening of the navigation channel for more than 5 m (Fig. 5c).

4.2 Modeling the impacts of the DNCP on hydrodynamics and sediment transport

The flow and sediment transport fields with and without the training walls obtained by process-based simulations show characteristic differences (Fig. 6). The significant changes after the DNCP are identified within the North Passage, where the flow pattern is changed from rotating to reciprocating as indicated by the modeled feathers of tidal currents (Fig. 6a, c). This is also found by a previous modeling study (Hu and Ding, 2009). The flow features indicate that the flow pattern at the EHS is also changed from rotating to reciprocating with decreased flow velocity after the DNCP (Fig. 6a, c). This implies that the training walls induce weaker tidal current and longer tidal slack period. Besides, the tidal currents at the seaward end of the South and North Passage, corresponding to the erosion zone, are enhanced by the training walls, while the flow pattern remains almost unchanged (Fig. 6a, c). Bed-level changes in estuarine area are determined by the gradient of the residual sediment transport. The modeled monthly-averaged sediment flux without the training walls indicates positive gradient of residual sediment transport from the ESH to the North Channel suggesting erosion at the ESH (Fig. 6b). By contrast, negative gradient from the North Passage to the EHS with the training wall implies accretion at the later area (Fig. 6d). The gradient of residual sediment transport at the seaward end of the North and South Passage is enhanced resulting from the presence of the training walls. The eroded sediment from the northern and southern erosion zone is converged by a sediment transport circulation system and transported into the North Passage with a much higher amount due to the training walls (Fig. 6b, d).

The differences of bed shear stress between numerical model runs are presented since sediment deposition or erosion processes are largely influenced by the bed shear stress (Fig. 7). The training walls cause decrease of the bed shear stress at the EHS at both flood and ebb maximum, while the bed shear stress at the seaward end of the North and South Passage is significantly enhanced only during rising tides (

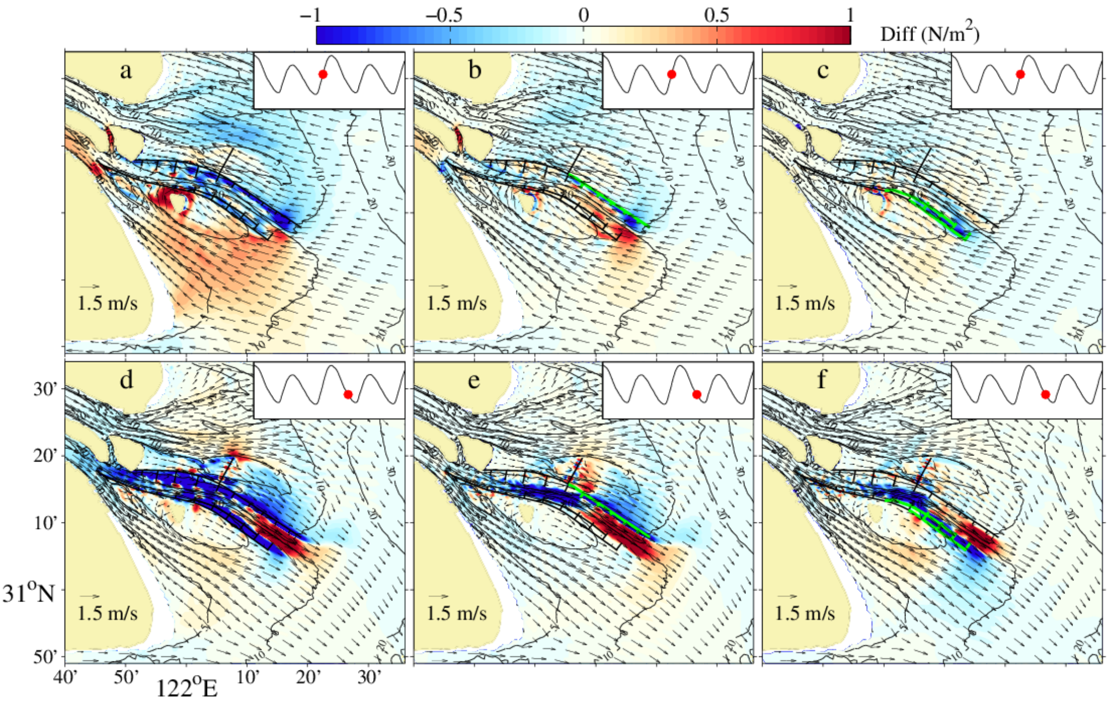

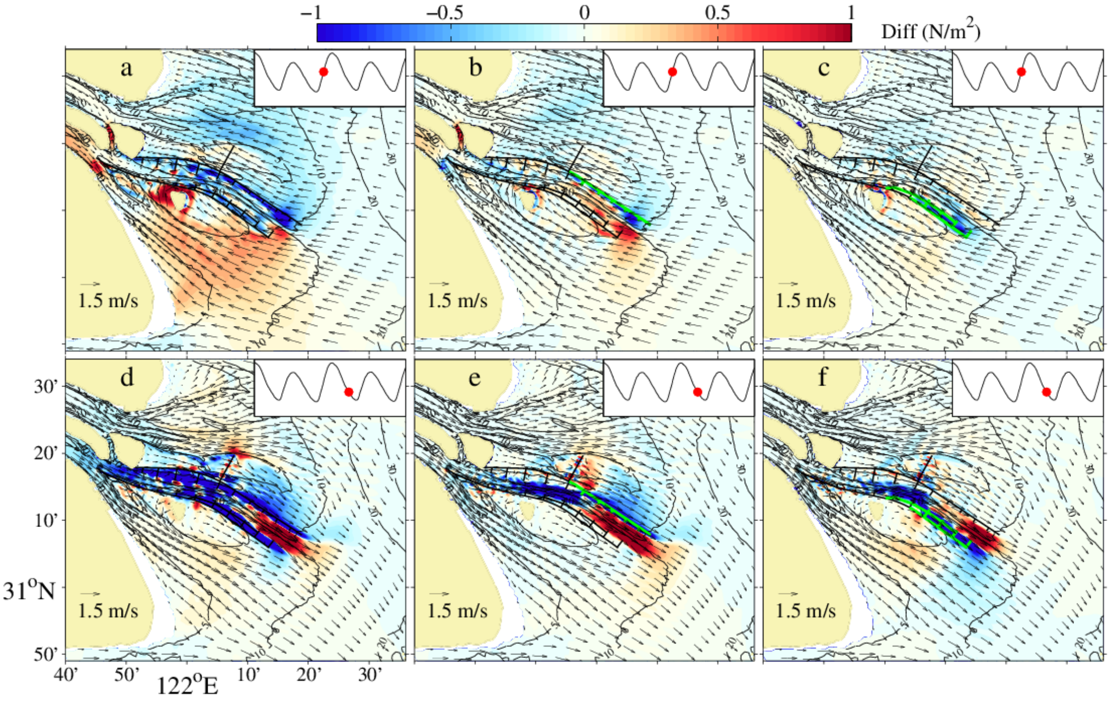

Fig. 7a, d). Modeling the impacts of the north dike shows similar results including the decrease at the EHS and increase at the southern erosion zone (

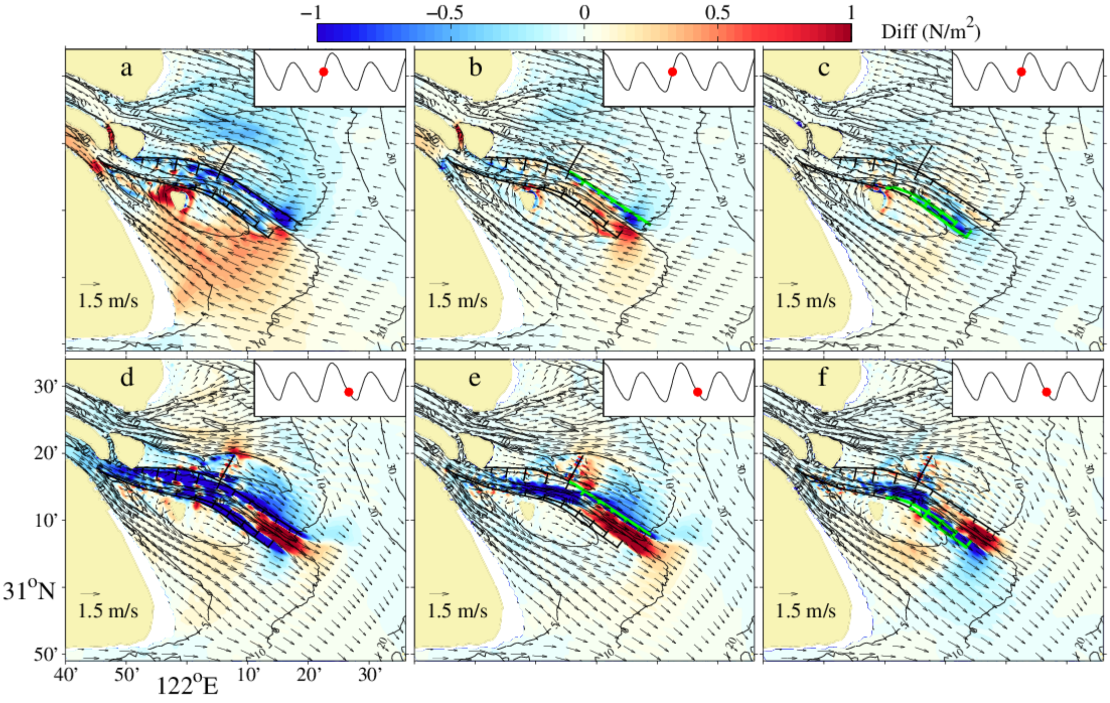

Fig. 7b, e). Moreover, the south dike results in limited impacts on the EHS and slightly decrease of the bed shear stress in the southern area (

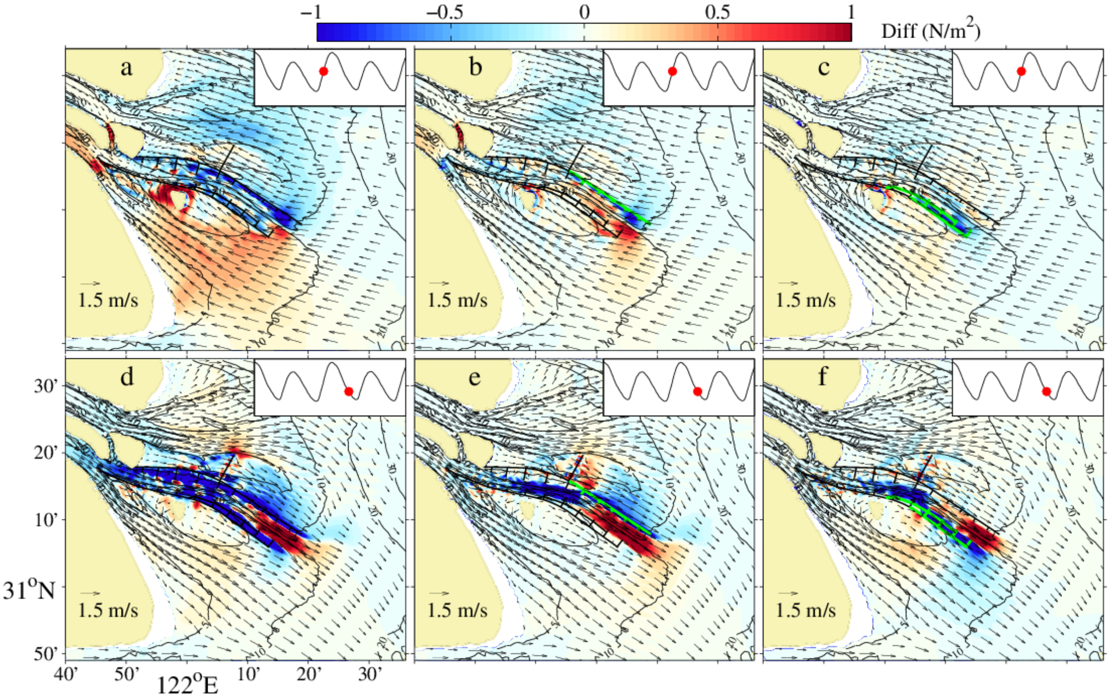

Fig. 7c, f).

4.3 Modeling the impacts of the DNCP on morphological changes

The modeled morphological changes under different configurations of the dikes and groynes provide direct evidence for the morphological impacts of the DNCPs (Fig. 8). The modeled and observed bed-level changes of the mouth bar area show qualitative agreement as described by Luan et al. (2017). Specifically, the accretion at the EHS and the erosion zones at the subaqueous delta are reproduced (Fig. 8a, b), which certifies the hindcast modeling as a reference case for investigating the observed evolution patterns at these areas. The difference between model runs with and without the training walls (Fig. 8c) is remarkable within the North Passage, including strong accretion within the dike-sheltered areas and erosion along the main channel due to the enhanced ebb flow. Excessive erosion at the entrance of the South

Passage is presented as the tidal currents are increased by the channel width narrowing and the increase of flow diversion ratio. Notably, the model run with training walls produces more accretion at the EHS which is identical with the location of the observed accretion zone at the EHS. Moreover, erosion at the seaward end of the North and South Passage is enhanced after including the training walls in the model. This area is consistent with the southern erosion zone of the subaqueous delta. Similar results are obtained in numerical experiment on the eastern half of the north dike, i.e. enhanced accretion at the EHS and erosion at the seaward end of the North and South Passage (Fig. 8d). However, the patterns at these two areas are absent in the results of the numerical experiment on the eastern half of the south dike which only produces slight accretion at the southern erosion zone (Fig. 8e). It is suggested that the impact of the south dike is limited relative to the north dike.

5. Discussion

5.1 Conversion from accretion to erosion due to river sediment reduction

The seaward part of the mouth bar area, which is defined as the study area for quantifying morphological changes, has converted from accretion to overall erosion during the period 1997-2013. This is consistent with the decreasing trend of the river sediment discharge (Fig. 2) and a previous study by Yang et al. (2011). The mean sediment discharge in the first decade after the TGD is less than 30% of the value in 1950s-1960s (Yang et al., 2015). River sediment reduction results in decrease of the suspended sediment concentration (SSC) in the estuarine area (Li et al., 2012; Liu et al., 2014). Based on statistical analysis of measurements, Li et al. (2012) concluded that the mean surface SSC over the past 10-20 years has decreased by 20-30% in the mouth bar area, which is lower than the 55% decrease in the inner estuary. The period coincides with the morphological evolution analysed in this study. Luan et al. (2016) suggested that the inner estuary has altered from deposition to erosion since 1980s, while present study indicates that the alteration in the seaward part of the mouth bar area occurs in the recent decade (Fig. 4c).

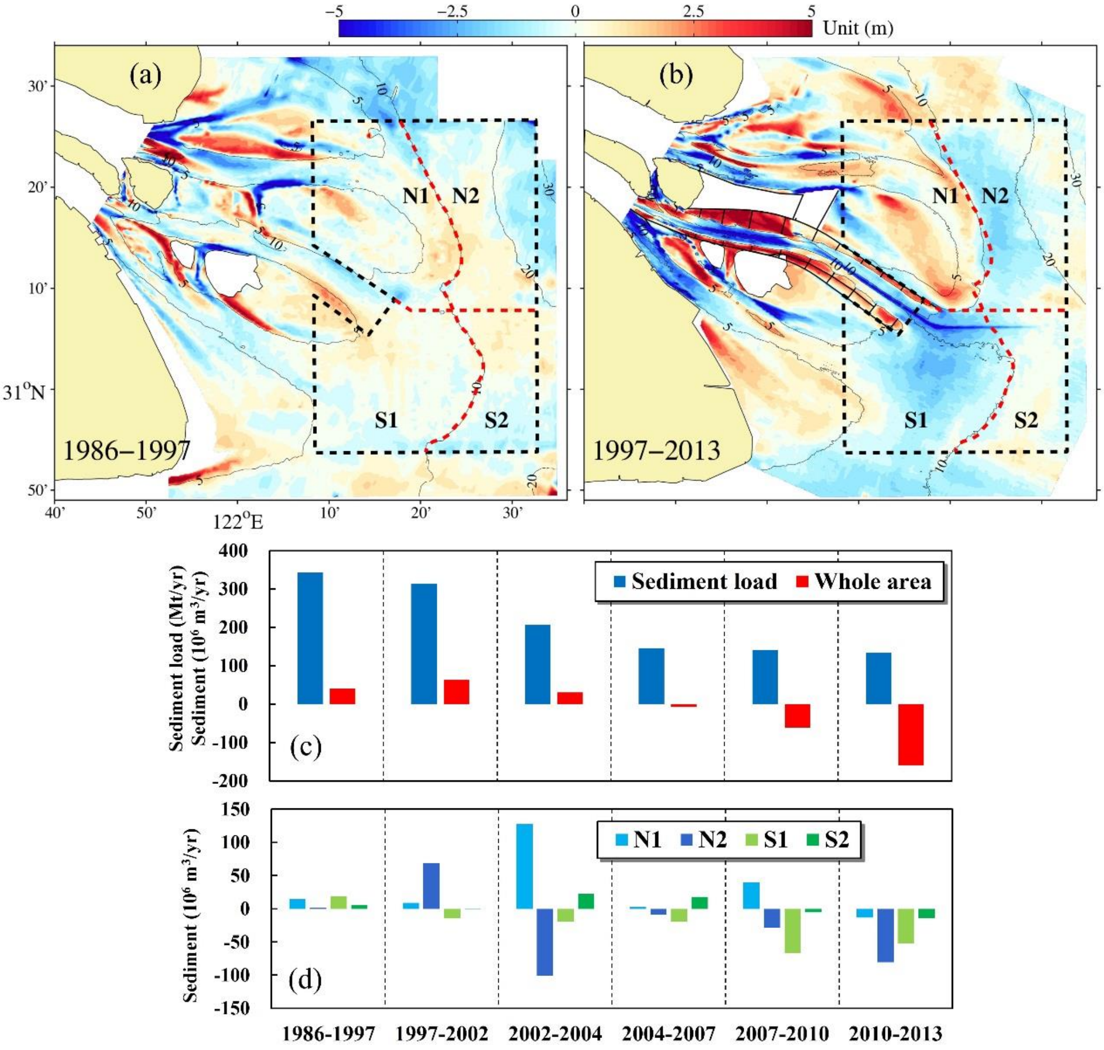

The Yangtze subaqueous delta behaves as a depocenter which is estimated to accumulate more than 40% of the fluvial sediment in the past millennia (Milliman et al., 1985; Liu et al., 2007), resulting in nearly 50 m of modern sediment at the mouth (Stanley and Chen, 1993). Therefore, the accretion rate of the mouth bar area deceased first as the sediment load started to decline in the 1980s, and the SSC within this area probably showed no apparent change. With the continuous river sediment decline, abundant bed sediment turned to compensate the decreasing SSC by erosion. Once the sediment load dropped below a critical level (Yang et al., 2003), the SSC in the mouth bar area started to decline which in turn intensified the erosion. This may explain that overall erosion of the whole study area occurred in 2010-2013 as the river sediment discharge remained a low value (Fig. 3e2; Fig. 4d). Li et al. (2012) also reported that the mean surface SSC in the north of the

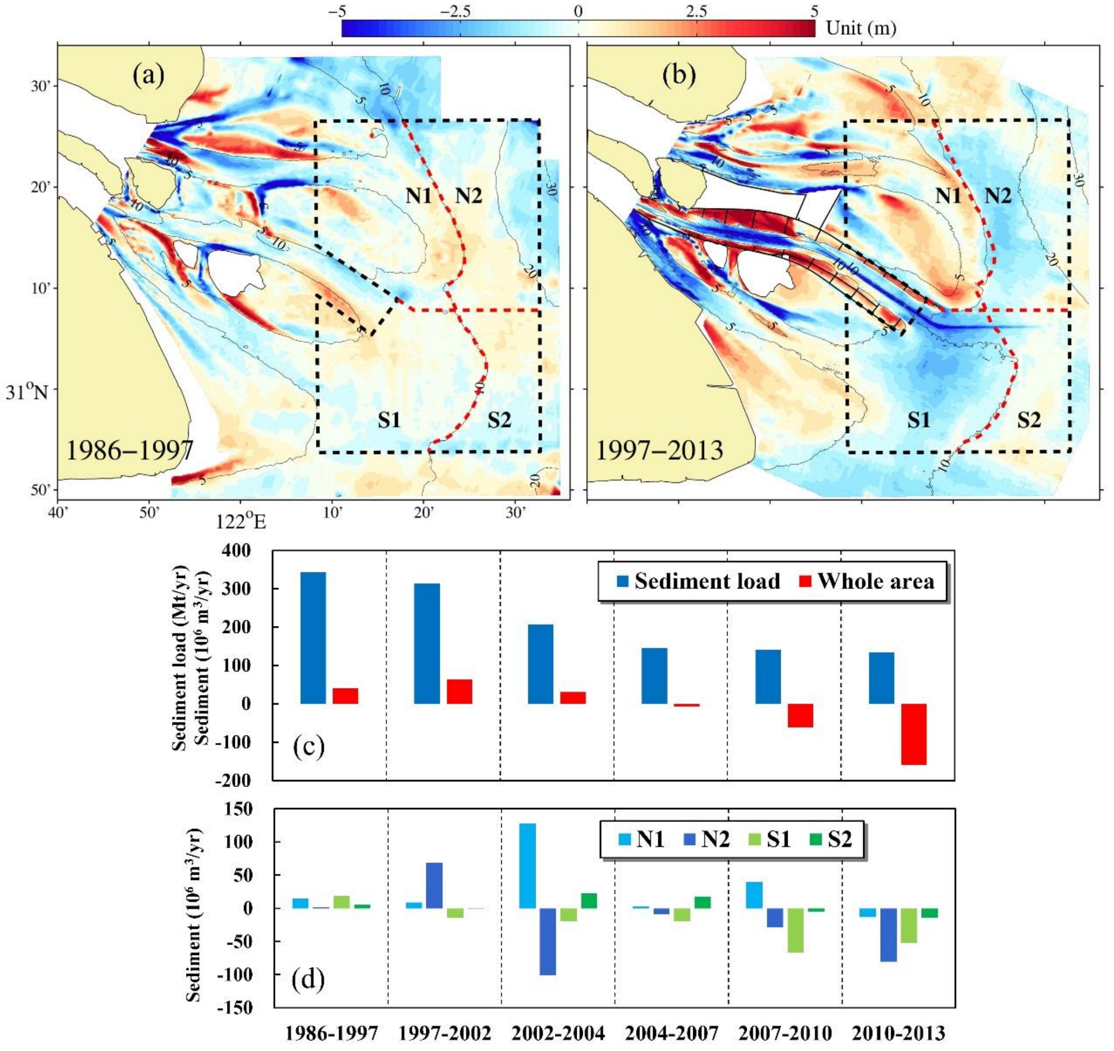

mouth bar area showed much lower decrease rate (e.g., 5% at Sheshan Station) than the south (e.g., 30% at Dajishan Station). This suggests that more bed sediment in the north is resuspended to partly offset the SSC decrease, and may explain more erosion in the Area N2 than the Area S1 (Fig. 4d).

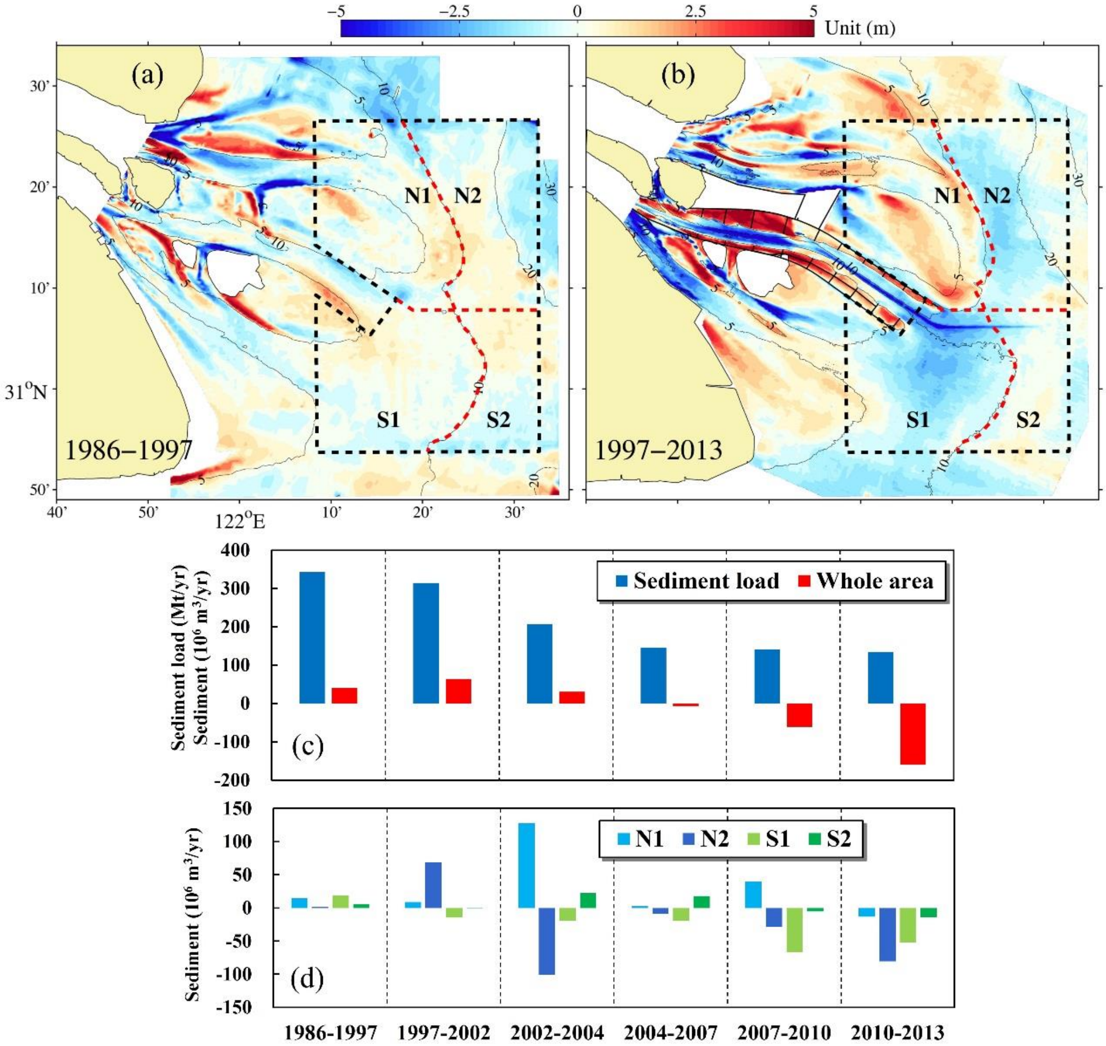

Generally, delta progradation or regression depends on the sediment budget between fluvial supply and offshore dispersal (Syvitski and Saito, 2007; Canestrelli et al., 2010). Under decreasing river sediment supply and relatively stable dispersal amount by coastal currents (Deng et al., 2017), the erosion of Yangtze subaqueous delta seems to be an inevitable tendency. Since the navigation channel and the North Passage between the twin dikes are excluded from the study area, the morphological changes of the open coastal waters as concerned show limited immediate impacts by training walls (e.g., rapid deposition in the dike-sheltered areas). Therefore, the decreasing river sediment supply is identified as the prime cause for the accretion-erosion conversion of the seaward part of the mouth bar area.

5.2 Distinct morphodynamic features due to the training walls

With the overall evolution pattern, morphodynamics of the Yangtze mouth bar area show distinct spatiotemporal variations during 1997-2013. One remarkable feature is the enhanced accretion at the EHS (

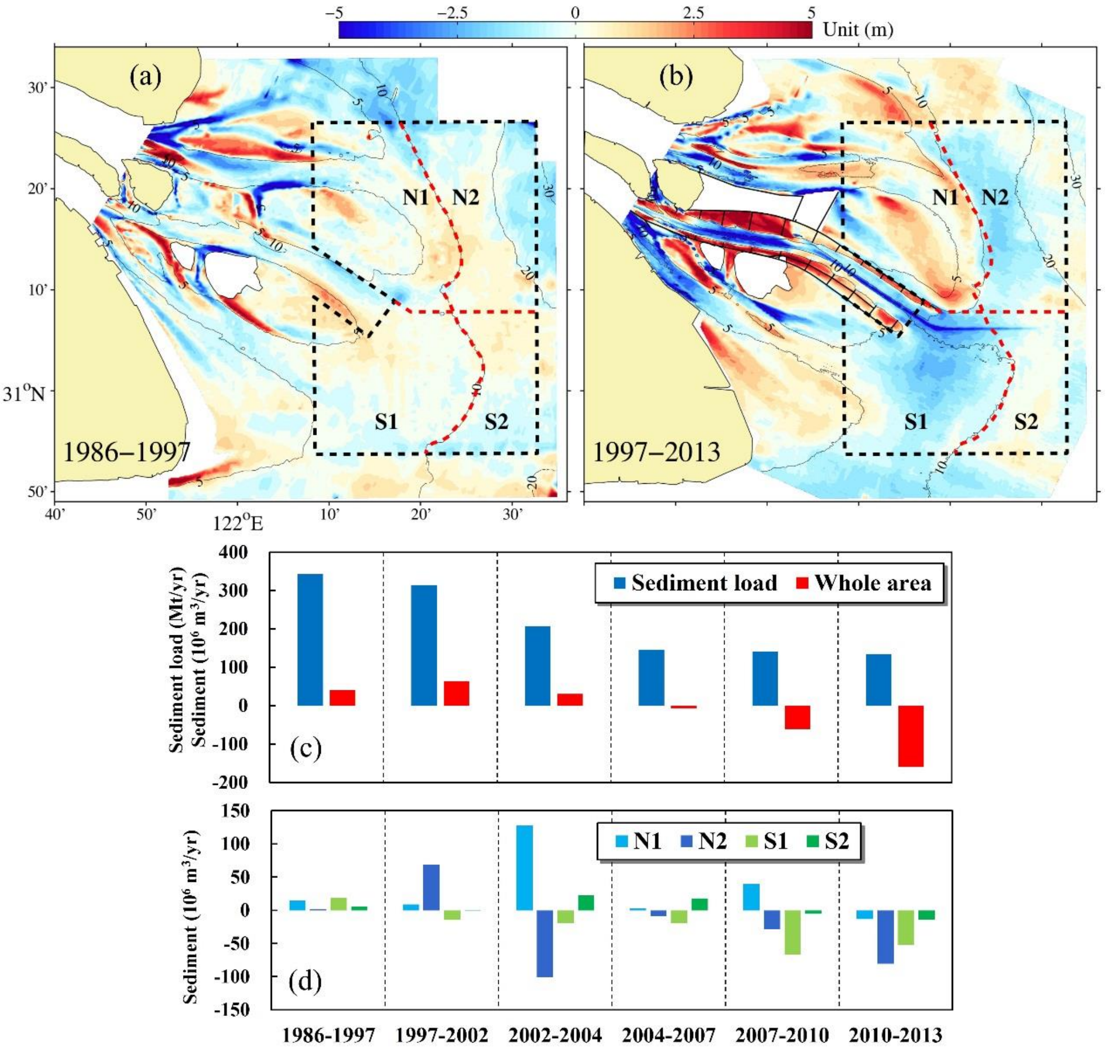

Fig. 4b), which is inconsistent with the evolution trend of the whole study area. As indicated by the hydrodynamic and morphological modeling results, the reciprocating flow pattern with weaker tidal current and longer slack period at the EHS after the construction of dikes implies a depositional environment. This is verified by the observed continuous accretion of the EHS in 1997-2010. Particularly, the peak of the accretion amount occurred in 2002-2004 during which the dikes were extended to the present location in Phase II (Fig. 1c). Though the SSC around the mouth bar area showed decreasing trend, the suspended sediment transported by the flood currents was easier to settle and accumulate at the EHS. Thus, the EHS converted to a sediment-starved status after the DNCP. Moreover, the accretion peak of

the EHS occurred simultaneously with the erosion peak of the northern erosion zone (Fig. 4d). The modeled sediment flux indicates that the eroded sediment at the subaqueous delta could be the important source for the accretion at the EHS under decreasing SSC. In sum, the enhanced accretion at the EHS was caused by the training walls along the North Passage, particularly the north dike, which changed the hydrodynamics and sediment transport patterns around the EHS.

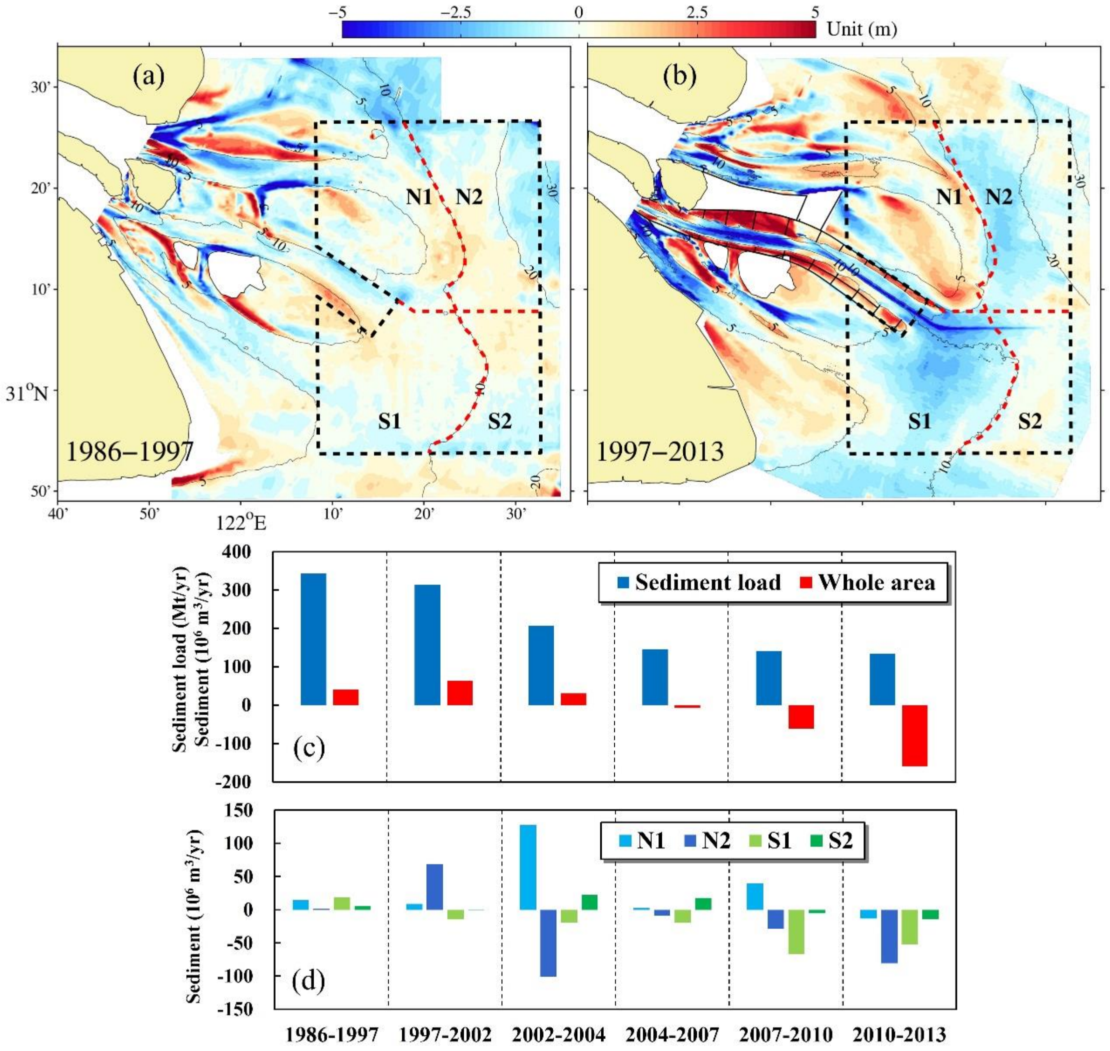

Another evolution feature is the formation of the erosion zones at the subaqueous delta (

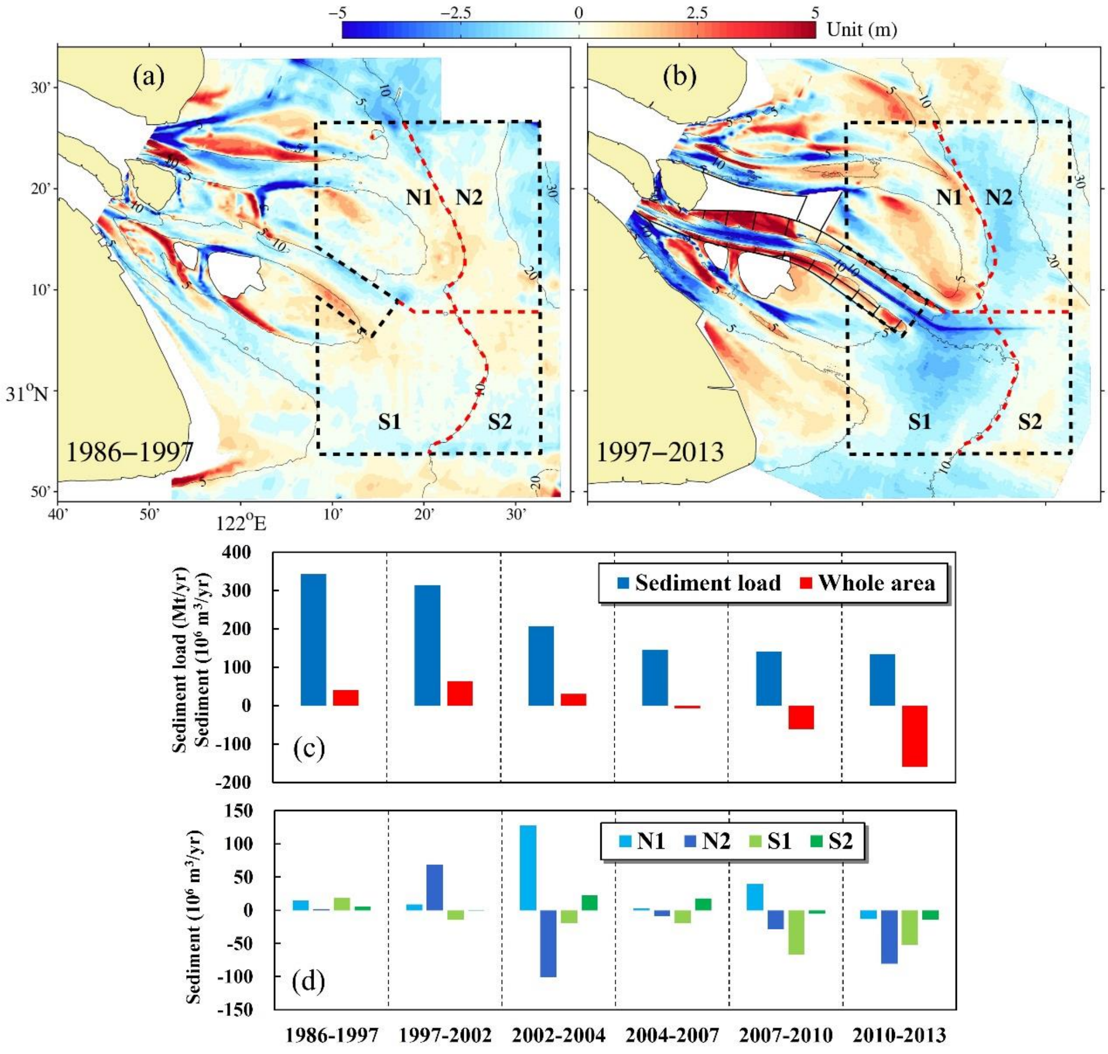

Fig. 4b). Though the Yangtze delta erosion is controlled by the river sediment reduction as discussed previously, it can be influenced by large-scale estuarine engineering projects. Model results demonstrate that the training walls enhance the hydrodynamic condition at the southern erosion zone during flood tide, and that the enhancement is mainly attributed to the presence of the north dike (Fig. 7). Subsequently, the modeled bed level changes show stronger erosion at the southern erosion zone due to the training walls (Fig. 8c, d). It is notable that the erosion zones at the subaqueous delta are the estuarine muddy areas where the seabed is mainly composed of unconsolidated fine-grained sediment (Fig. S3). These muddy areas are subject to intensive sediment exchange between the water column and seabed

through sediment deposition and resuspension (Liu et al., 2010). Therefore, bed level changes of these areas are more sensitive to variations of the SSC and hydrodynamic condition than other areas covered by coarser sediment. The muddy areas are likely to involve the earliest erosion in the subaqueous delta in response to the decreasing river sediment supply, and the erosion is accelerated after the construction of the training walls, especially the north dike.

Based on the morphological evolution analysis and numerical simulations above, the sediment transport paths and specific erosion/deposition locations within the study area before and after the DNCP are schematized as shown in Fig. 9. Before the DNCP in 1997, the north part of the mouth bar area was under accretion with higher accretion rate at the mouth of the North Channel than the EHS, while erosion has occurred at the seaward end of the North and South Passage (Fig. 9a). The eroded sediment was involved in a circulation system and was partly delivered to the outer sea by tidal currents. After the DNCP, suspended sediment driven by tidal currents tended to deposit at the EHS after the north dike was extended to its present location. Thereby, accretion at the EHS was largely enhanced (Fig. 9b). Meanwhile, the mouth of the North Channel converted from accretion to strong erosion, which is regarded as the northern erosion zone within the study area (

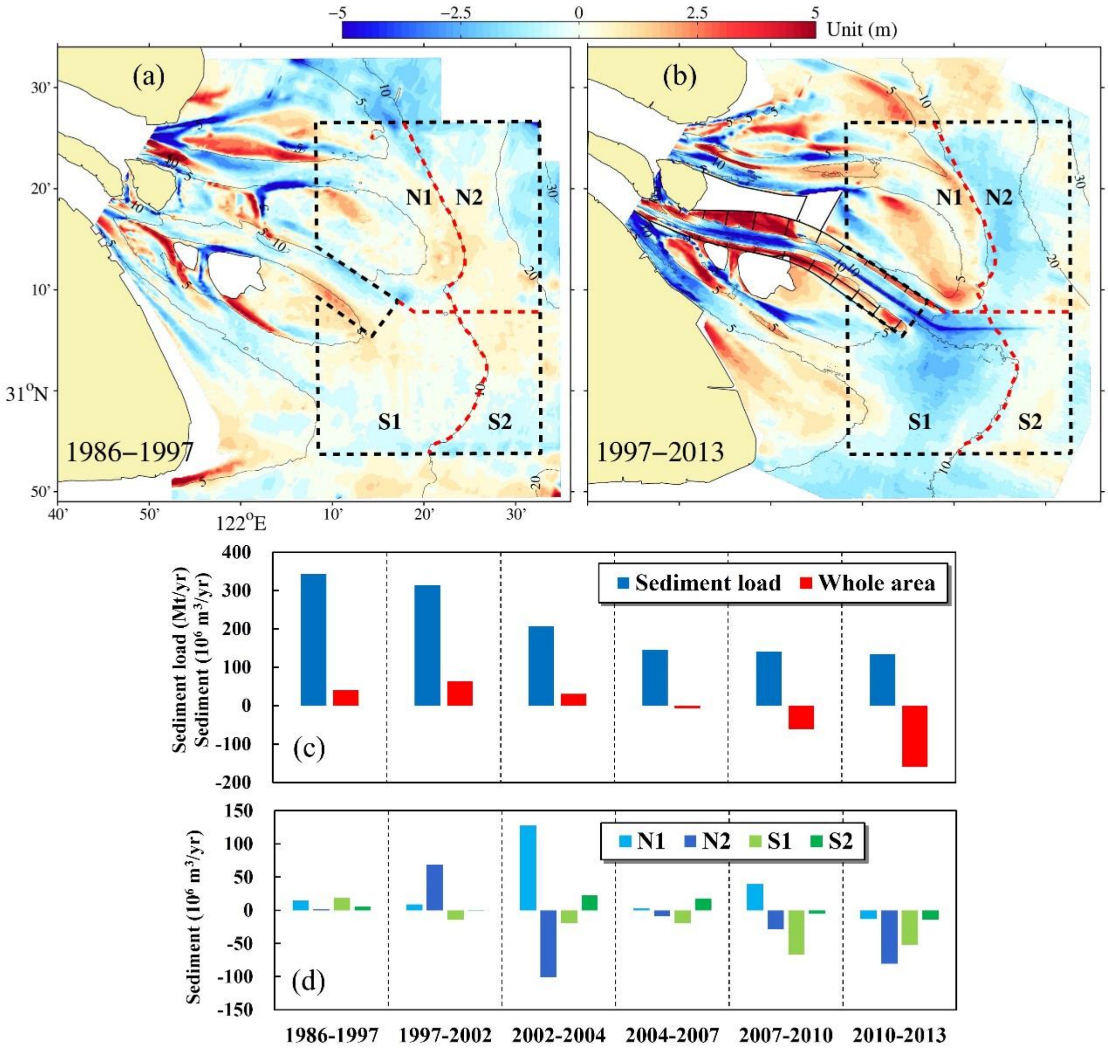

Fig. 4b). Erosion at the seaward end of the North and South Passage was enhanced by the training walls superimposed upon the river sediment reduction. Part of the eroded sediment from both erosion zones was combined and transported away to the outer sea, while the rest passed across the south dike and may become a considerable source for back-siltation of the navigation channel along the North Passage (Zhu et al., 2016).

5.3 Implications for deltaic morphodynamic equilibrium and sustainability

A widely concerned issue for deltaic morphodynamics is the equilibrium morphological configurations and the timescale to approach them in response to natural forcing changes and human interventions (Zhou et al., 2017). Under sufficient sediment supply, the morphodynamic equilibrium of a propagating river delta usually refers to its growth limit. Gao (2007) suggested that the growth limit of the Yangtze delta is constrained by multiple factors, including the original bathymetry, sediment supply and retention, sea-level rise and bed subsidence. Conceptual geometric models proposed by Gao (2007) indicates that the Yangtze Delta will reach its growth limit in the near future under river sediment reduction. Controlled by the variation of sediment discharge, the Yangtze subaqueous delta experienced rapid accretion in 1950s-1960s, decreased accretion since 1980s and regional erosion in the recent decade (Yang et al., 2011; Dai et al., 2014; Luan et al., 2016). Though the sediment load remained relatively stable at a low level (~140 Mt yr^{-1}) after 2004 (Fig. 2), the net erosion amount of the study area increased almost linearly (

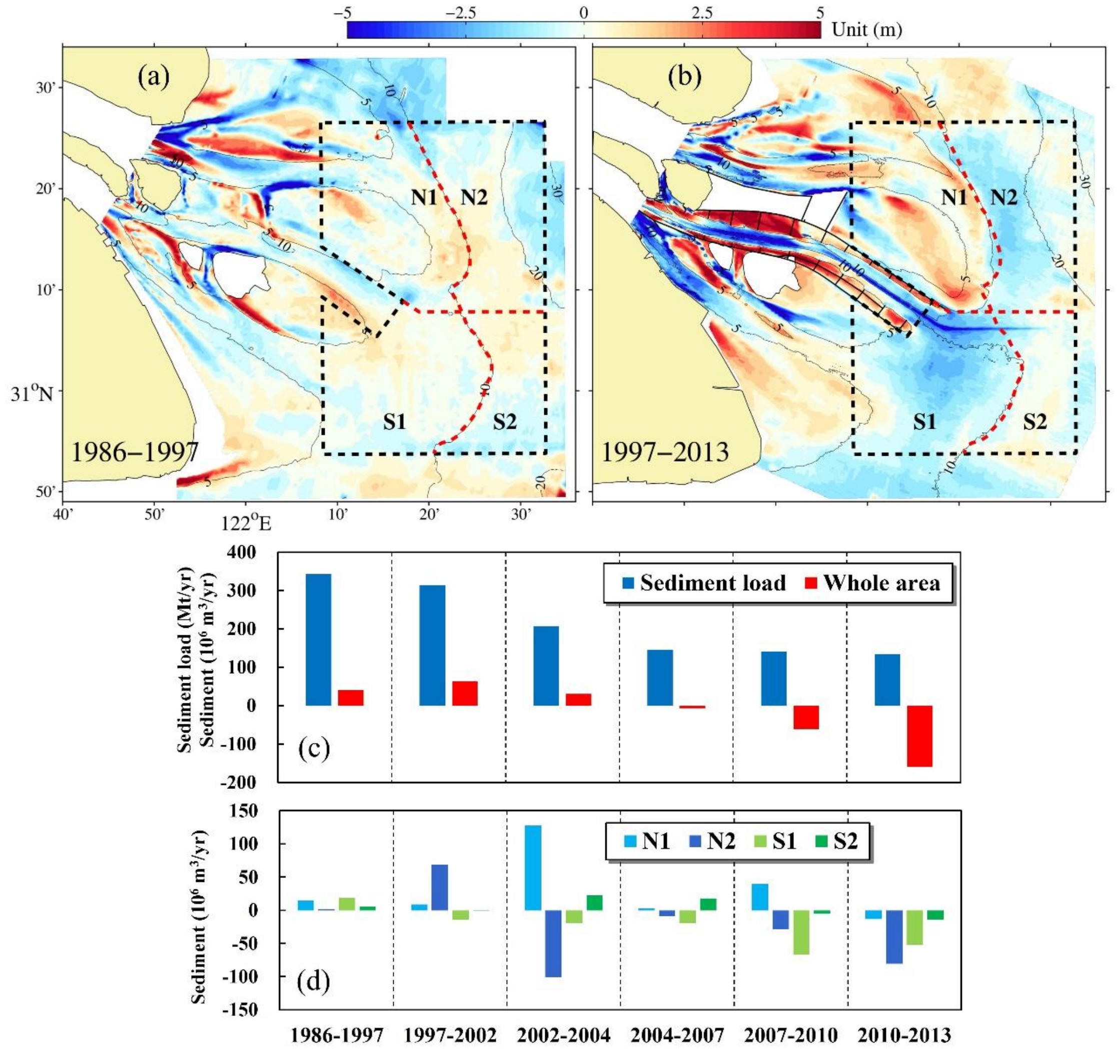

Fig. 4c) until the 2010-2013 when all the four sub-areas were under net erosion in 2010-2013, which is just the opposite of net accretion of four sub-areas in 1986-1997. On the one hand, this is probably because the sediment discharge had already dropped below a critical value for converting from accretion to erosion, and the fine-grained sediment within the muddy areas was continuously eroded to compensate the decreasing SSC. This also explains the time lag between the decrease in SSC within the estuarine waters and the decrease in sediment discharge (Li et al., 2012). On the other hand, the training walls along the North Passage enhanced the erosion at the southern erosion zone (Fig. 8c). Thus it can be concluded that the Yangtze subaqueous delta is accelerating to approach the morphodynamic

equilibrium due to the impacts of large-scale estuarine engineering projects.

Considering that the observed erosion zones contain abundant fine-grained sediment, the present erosion thickness has not yet reached the maximum, and deepening is likely to continue in the future until the dynamic equilibrium. The erosion limit and timescale for approaching to the equilibrium is determined by balance between the decreasing erosional ability of tidal currents due to continuous deepening and increasing anti-erosional ability of the seabed due to armoring and increased compaction of deeper sediment. According to the variation of hypsometry curves, the sub-area N2 converted from accretion to erosion around the year 2002. The area deeper than 20 m within the N2 in 2013 returned to nearly the same value in 1997, while the area shallower than 20 m in 2013 has already showed net erosion relative to the year 1997. It is suggested that deeper area is less sensitive to the conversion from accretion to erosion, and that the deeper subaqueous delta may reach the equilibrium in an earlier stage.

Similar situations can also be found in other estuarine and coastal areas around the world. Generally, the timescale for estuaries and deltas towards a new morphodynamic equilibrium after human interventions is determined by hydrodynamic condition (e.g., tide, wave, and river flow), sediment supply and property, and geological and landform setting of the systems. The Mersey Estuary, a tidal dominant estuary on the west coast of the UK, experienced significant accretion in 1906-1977 due to the construction of training walls and dredging activity, and evolved towards an equilibrium estuary state over a period of approximately 70 years (Thomas et al., 2002). The construction of a large-scale closure dam (Afsluitdijk) in the Dutch Wadden Sea in 1932 has disturbed the equilibrium condition of adjacent tidal basins, which are still adapting to the human intervention after nearly 80 years and on the way to a new dynamic equilibrium state (Elias et al., 2003; Dastgheib et al., 2008). The Eastern Scheldt estuary showed overall erosion at the ebb-tidal delta and tidal flats within the estuary after the construction of the storm surge barrier in 1986 (Eelkema et al., 2013; Wang et al., 2015; de Vet et al., 2017), and the estuary is far from any kind of equilibrium at present (Eelkema et al., 2013). The responding time of the Yangtze subaqueous delta to large-scale estuarine engineering projects remains unknown and merits further systematic research.

Among the global dataset of deltas, the Yangtze delta is a typical example under interactive impacts of river input changes and human activities (Syvitski et al., 2009; Tessler et al., 2015). Day et al. (1997, 2016) considered delta sustainability from geomorphic, ecological, and economic perspectives. The geomorphic functioning and sustainability of the Yangtze subaqueous delta can be affected by large-scale estuarine engineering projects. For instance, the continuous erosion at the subaqueous delta may cause engineering failure and increase the exposure risk of buried oil/gas pipelines. Another example is the EHS which is proposed to build an excavated harbor basin to meet the increasing shipping demand (Ding and Li, 2013). Though the dike-induced accretion at the EHS is favorable for the harbor construction, net erosion was observed at the EHS after 2010. Therefore, Yangtze delta sustainability calls for continuous bathymetry observation and reliable prediction on future evolution trend of the mouth bar area under continuous decrease in sediment discharge as predicted (Yang et al., 2014).

6. Conclusions

This study addresses the morphodynamic evolution processes of the mouth bar area of the Yangtze Estuary in 1997-2013 using observed bathymetric data. The results reveal that the seaward part of the mouth bar area, defined as the study area for calculation of sediment volume change, converted from net accretion to net erosion around the year 2004. The prime cause for this conversion is the river sediment reduction, which induced the decrease in SSC around the mouth bar area and thereby sediment compensation of the subaqueous delta by erosion. Though the sediment discharge remained relatively stable at a low level (~140 Mt yr^{-1}) after 2004, the erosion rate of the study area increased almost linearly, suggesting that the erosion were accelerating. The erosion/deposition patterns of the study area show distinct spatial variations during the period 1997-2013. Specifically, an erosion zone formed at the mouth of the North Channel after 2002 with the erosion rate peak in 2002-2004 and the overall erosion thickness nearly 2 m. Another erosion zone formed at the seaward end of the North and South Passage after 1997 with increasing erosion rate and larger overall erosion thickness than the northern one. The erosion volumes of both the northern and southern erosion zones increased gradually after 2004. Meanwhile, the EHS involved abnormal accretion under the trend of decreasing sediment discharge, especially the strongest accretion in 2002-2004. The net accretion status of the EHS was retained until 2010.

Process-based modeling approach (Delft3D) is applied to investigate the morphological impacts of large-scale estuarine engineering projects on the mouth bar area, considering that the study period of morphological evolution coincides with the construction period of the DNCP along the North Passage (1997-2010). Hydrodynamic simulations indicate that the training walls change the flow pattern at the EHS from rotating flows to reciprocating flows with decreased flow velocity, particularly decrease the bed shear stress at the EHS during ebb tide. Longer tidal slack period and weaker hydrodynamic condition characterize the EHS as a depositional environment, which is consistent with the modeled sediment flux. The flow pattern at the southern erosion zone shows no evident change after the DNCP, whereas the tidal flows are enhanced as reflected by larger bed shear stress during flood tide. Morphological modeling results show that the training walls enhanced the accretion at the EHS and erosion at the southern erosion zone, and these impacts are primarily contributed by the north dike. This can also verified by the extension of the twin dikes to the present locations in Phase II (2002-2004) and simultaneous accretion peak of the EHS. The Yangtze subaqueous delta is accelerating towards the morphodynamic equilibrium under large-scale estuarine engineering projects superimposed with river sediment reduction. The timescale for approaching to the erosion limit remained unknown, and calls for further systematic research to support the sustainable management of this large-scale estuarine system.

Acknowledgments

This study is financed by…

References

Anthony, E.J., Brunier, G., Besset, M., Goichot, M., Dussouillez, P., Nguyen, V.L., 2015. Linking rapid erosion of the Mekong River delta to human activities. Sci. Rep.-UK 5, 14745.

Blott, S.J., Pye, K., van der Wal, D., Neal, A., 2006. Long-term morphological change and its causes in the Mersey Estuary, NW England. Geomorphology 81, 185-206.

Blum, M.D., Roberts, H.H., 2009. Drowning of the Mississippi Delta due to insufficient sediment supply and global sea-level rise. Nat. Geosci. 2, 488-491.

Canestrelli, A., Fagherazzi, S., Defina, A., Lanzoni, S., 2010. Tidal hydrodynamics and erosional power in the Fly River delta, Papua New Guinea. Journal of Geophysical Research: Earth Surface 115, F4033.

Chen, J., Zhu, H., Dong, Y., Sun, J., 1985. Development of the Changjiang estuary and its submerged delta. Cont. Shelf Res. 4, 47-56.

Chu, Z.X., Sun, X.G., Zhai, S.K., Xu, K.H., 2006. Changing pattern of accretion/erosion of the modern Yellow River (Huanghe) subaerial delta, China: Based on remote sensing images. Mar. Geol. 227, 13-30.

Coleman, J.M., Wright, L.D., 1975. Modern river deltas: variability of processes and sand bodies,in: Broussard, M.L. (Ed.), Deltas: Models for Exploration. Houston Geological Society, pp. 99-149.

Dai, Z., Liu, J.T., Fu, G., Xie, H., 2013. A thirteen-year record of bathymetric changes in the North Passage, Changjiang (Yangtze) estuary. Geomorphology 187, 101-107.

Dai, Z., Liu, J.T., Wei, W., Chen, J., 2014. Detection of the Three Gorges Dam influence on the Changjiang (Yangtze River) submerged delta. Sci. Rep.-UK 4, 6600.

Dastgheib, A., Roelvink, J.A., Wang, Z.B., 2008. Long-term process-based morphological modeling of the Marsdiep Tidal Basin. Mar. Geol. 256, 90-100.

Day, J., Hall, C.S., Kemp, W.M., Yanez-Aranciba, A., 1989. Estuarine Ecology. John-Wiley, New York.

Day, J.W., Martin, J.F., Cardoch, L., Templet, P.H., 1997. System functioning as a basis for sustainable management of deltaic ecosystems. Coast. Manage. 25, 115-153.

de Vet, P.L.M., van Prooijen, B.C., Wang, Z.B., 2017. The differences in morphological development between the intertidal flats of the Eastern and Western Scheldt. Geomorphology 281, 31-42.

De Vriend, H., Wang, Z., Ysebaert, T., Herman, P.J., Ding, P., 2011. Eco-Morphological Problems in the Yangtze Estuary and the Western Scheldt. Wetlands 31, 1033-1042.

Deng, B., Wu, H., Yang, S., Zhang, J., 2017. Longshore suspended sediment transport and its implications for submarine erosion off the Yangtze River Estuary. Estuarine, Coastal and Shelf Science 190, 1-10.

Ding, P.X., Li, S.G., 2013. Planning ideas and key technology for building excavated-in harbor basin in the Hengsha Shoal of the Yangtze Estuary. Journal of East China Normal University (Natural Sciences), 1-9 (in Chinese with English abstract).

Dissanayake, D.M.P.K., Wurpts, A., Miani, M., Knaack, H., Niemeyer, H.D., Roelvink, J.A., 2012. Modelling morphodynamic response of a tidal basin to an anthropogenic effect: Ley Bay, East Frisian Wadden Sea – applying tidal forcing only and different sediment fractions. Coast. Eng. 67, 14-28.

Eelkema, M., Wang, Z.B., Hibma, A., Stive, M.J., 2013. Morphological effects of the Eastern Scheldt storm surge barrier on the ebb-tidal delta. Coast. Eng. J. 55, 1350010.

Elias, E., Stive, M.J.F., Bonekamp, H., Cleveringa, J., 2003. Tidal inlet dynamics in response to human intervention. Coast. Eng. J. 45, 629-658.

Ericson, J.P., Vörösmarty, C.J., Dingman, S.L., Ward, L.G., Meybeck, M., 2006. Effective sea-level rise and deltas: Causes of change and human dimension implications. Global Planet. Change 50, 63-82.

Gao, S., 2007. Modeling the growth limit of the Changjiang Delta. Geomorphology 85, 225-236.

Giosan, L., Syvitski, J., Constantinescu, S., Day, J., 2014. Climate change: protect the world's deltas. Nature 516, 31-33.

Guo, L., van der Wegen, M., Roelvink, J.A., He, Q., 2014. The role of river flow and tidal asymmetry on 1D estuarine morphodynamics. Journal of Geophysical Research: Earth Surface 119.

Hori, K., Saito, Y., Zhao, Q., Cheng, X., Wang, P., Sato, Y., Li, C., 2001. Sedimentary facies and Holocene progradation rates of the Changjiang (Yangtze) delta, China. Geomorphology 41, 233-248.

Hu, K., Ding, P., 2009. The Effect of Deep Waterway Constructions on Hydrodynamics and Salinities in Yangtze Estuary, China. J. Coastal Res., 961-965.

Lesser, G.R., Roelvink, J.A., van Kester, J.A.T.M., Stelling, G.S., 2004. Development and validation of a three-dimensional morphological model. Coast. Eng. 51, 883-915.

Li, P., Yang, S.L., Milliman, J.D., Xu, K.H., Qin, W.H., Wu, C.S., Chen, Y.P., Shi, B.W., 2012. Spatial, Temporal, and Human-Induced Variations in Suspended Sediment Concentration in the Surface Waters of the Yangtze Estuary and Adjacent Coastal Areas. Estuar. Coast. 35, 1316-1327.

Liu, G., Zhu, J., Wang, Y., Wu, H., Wu, J., 2011. Tripod measured residual currents and sediment flux: Impacts on the silting of the Deepwater Navigation Channel in the

Changjiang Estuary. Estuarine, Coastal and Shelf Science 93, 192-201.

Liu, H., He, Q., Wang, Z., Weltje, G.J., Zhang, J., 2010. Dynamics and spatial variability of near-bottom sediment exchange in the Yangtze Estuary, China. Estuarine, Coastal and Shelf Science 86, 322-330.

Liu, J.H., Yang, S.L., Zhu, Q., Zhang, J., 2014. Controls on suspended sediment concentration profiles in the shallow and turbid Yangtze Estuary. Cont. Shelf Res. 90, 96-108.

Liu, J.P., Xu, K.H., Li, A.C., Milliman, J.D., Velozzi, D.M., Xiao, S.B., Yang, Z.S., 2007. Flux and fate of Yangtze River sediment delivered to the East China Sea. Geomorphology 85, 208-224.

Luan, H.L., Ding, P.X., Wang, Z.B., Ge, J.Z., 2017. Process-based morphodynamic modeling of the Yangtze Estuary at a decadal timescale: Controls on estuarine evolution and future trends. Geomorphology 290, 347-364.

Luan, H.L., Ding, P.X., Wang, Z.B., Ge, J.Z., Yang, S.L., 2016. Decadal morphological evolution of the Yangtze Estuary in response to river input changes and estuarine engineering projects. Geomorphology 265, 12-23.

Luo, X.X., Yang, S.L., Wang, R.S., Zhang, C.Y., Li, P., 2017. New evidence of Yangtze delta recession after closing of the Three Gorges Dam. Sci. Rep.-UK 7.

Luo, X.X., Yang, S.L., Zhang, J., 2012. The impact of the Three Gorges Dam on the downstream distribution and texture of sediments along the middle and lower Yangtze River (Changjiang) and its estuary, and subsequent sediment dispersal in the East China Sea. Geomorphology 179, 126-140.

Milliman, J.D., Farnsworth, K.L., 2013. River discharge to the coastal ocean: a global synthesis. Cambridge University Press, Cambridge.

Milliman, J.D., Shen, H.T., Yang, Z.S., Mead, R.H., 1985. Transport and deposition of river sediment in the Changjiang estuary and adjacent continental shelf. Cont. Shelf Res. 4, 37-45.

Milliman, J.D., Yun-Shan, Q., Mei-E, R., Saito, Y., 1987. Man's Influence on the Erosion and Transport of Sediment by Asian Rivers: The Yellow River (Huanghe) Example. The Journal of Geology 95, 751-762.

Morton, R.A., Bernier, J.C., Barras, J.A., Ferina, N.F., 2005. Rapid subsidence and historical wetland loss in the Mississippi delta plain: likely causes and future implications, US Geol. Surv., Washington, DC.

Renaud, F.G., Syvitski, J.P., Sebesvari, Z., Werners, S.E., Kremer, H., Kuenzer, C., Ramesh, R., Jeuken, A., Friedrich, J., 2013. Tipping from the Holocene to the Anthropocene: How threatened are major world deltas? Curr. Opin. Env. Sust. 5, 644-654.

Roelvink, J.A., 2006. Coastal morphodynamic evolution techniques. Coast. Eng. 53, 277-287.

Sanchez-Arcilla, A., Jimenez, J.A., Valdemoro, H.I., 1998. The Ebro Delta: Morphodynamics and Vulnerability. J. Coastal Res. 14, 755-772.

Stanley, D.J., 1996. Nile delta: extreme case of sediment entrapment on a delta plain and consequent coastal land loss. Mar. Geol. 129, 189-195.

Stanley, D.J., Chen, Z., 1993. Yangtze delta, eastern China: 1. Geometry and subsidence of Holocene depocenter. Mar. Geol. 112, 1-11.

Stanley, D.J., Warne, A.G., 1994. Worldwide Initiation of Holocene Marine Deltas by

Deceleration of Sea-Level Rise. Science 265, 228-231.

Su, M., Yao, P., Wang, Z.B., Zhang, C.K., Stive, M.J.F., 2016. Exploratory morphodynamic hindcast of the evolution of the abandoned Yellow River delta, 1578-1855 AD. Mar. Geol.

Syvitski, J.P.M., 2008. Deltas at risk. Sustain. Sci. 3, 23-32.

Syvitski, J.P.M., Kettner, A., 2011. Sediment flux and the Anthropocene. Phil. Trans. R. Soc. A 369, 957-975.

Syvitski, J.P.M., Kettner, A.J., Overeem, I., Hutton, E.W.H., Hannon, M.T., Brakenridge, G.R., Day, J., Vorosmarty, C., Saito, Y., Giosan, L., Nicholls, R.J., 2009. Sinking deltas due to human activities. Nat. Geosci. 2, 681-686.

Syvitski, J.P.M., Saito, Y., 2007. Morphodynamics of deltas under the influence of humans. Global Planet. Change 57, 261-282.

Syvitski, J.P.M., Vörösmarty, C.J., Kettner, A.J., Green, P., 2005. Impact of Humans on the Flux of Terrestrial Sediment to the Global Coastal Ocean. Science 308, 376-380.

Tessler, Z.D., Vörösmarty, C.J., Grossberg, M., Gladkova, I., Aizenman, H., Syvitski, J.P.M., Foufoula-Georgiou, E., 2015. Profiling risk and sustainability in coastal deltas of the world. Science 349, 638-643.

Thomas, C.G., Spearman, J.R., Turnbull, M.J., 2002. Historical morphological change in the Mersey Estuary. Cont. Shelf Res. 22, 1775-1794.

Tian, B., Zhou, Y., Thom, R.M., Diefenderfer, H.L., Yuan, Q., 2015. Detecting wetland changes in Shanghai, China using FORMOSAT and Landsat TM imagery. J. Hydrol. 529, 1-10.

van der Wegen, M., Jaffe, B.E., Roelvink, J.A., 2011. Process-based, morphodynamic hindcast of decadal deposition patterns in San Pablo Bay, California, 1856–1887. Journal of Geophysical Research: Earth Surface 116, F2008.

van Maren, D.S., van Kessel, T., Cronin, K., Sittoni, L., 2015. The impact of channel deepening and dredging on estuarine sediment concentration. Cont. Shelf Res. 95, 1-14.

Vörösmarty, C.J., Meybeck, M., Fekete, B., Sharma, K., Green, P., Syvitski, J.P.M., 2003. Anthropogenic sediment retention: major global impact from registered river impoundments. Global Planet. Change 39, 169-190.

Walling, D.E., 2006. Human impact on land–ocean sediment transfer by the world's rivers. Geomorphology 79, 192-216.

Wang, H., Yang, Z., Saito, Y., Liu, J.P., Sun, X., Wang, Y., 2007. Stepwise decreases of the Huanghe (Yellow River) sediment load (1950–2005): Impacts of climate change and human activities. Global Planet. Change 57, 331-354.

Wang, J., Baskaran, M., Hou, X., Du, J., Zhang, J., 2017. Historical changes in 239Pu and 240Pu sources in sedimentary records in the East China Sea: Implications for provenance and transportation. Earth Planet. Sc. Lett. 466, 32-42.

Wang, Z.B., Van Maren, D.S., Ding, P.X., Yang, S.L., Van Prooijen, B.C., De Vet, P.L.M., Winterwerp, J.C., De Vriend, H.J., Stive, M.J.F., He, Q., 2015. Human impacts on morphodynamic thresholds in estuarine systems. Cont. Shelf Res., R3681.

Wei, W., Tang, Z., Dai, Z., Lin, Y., Ge, Z., Gao, J., 2015. Variations in tidal flats of the Changjiang (Yangtze) estuary during 1950s–2010s: Future crisis and policy implication. Ocean Coast. Manage. 108, 89-96.

Wu, Z.Y., Saito, Y., Zhao, D.N., Zhou, J.Q., Cao, Z.Y., Li, S.J., Shang, J.H., Liang, Y.Y.,

2016. Impact of human activities on subaqueous topographic change in Lingding Bay of the Pearl River estuary, China, during 1955 – 2013. Sci. Rep.-UK 6, 37742.

Yang, S.L., Belkin, I.M., Belkina, A.I., Zhao, Q.Y., Zhu, J., Ding, P.X., 2003. Delta response to decline in sediment supply from the Yangtze River: evidence of the recent four decades and expectations for the next half-century. Estuarine, Coastal and Shelf Science 57, 689-699.

Yang, S.L., Milliman, J.D., Li, P., Xu, K., 2011. 50,000 dams later: Erosion of the Yangtze River and its delta. Global Planet. Change 75, 14-20.

Yang, S.L., Milliman, J.D., Xu, K.H., Deng, B., Zhang, X.Y., Luo, X.X., 2014. Downstream sedimentary and geomorphic impacts of the Three Gorges Dam on the Yangtze River. Earth-Sci. Rev. 138, 469-486.

Yang, S.L., Xu, K.H., Milliman, J.D., Yang, H.F., Wu, C.S., 2015. Decline of Yangtze River water and sediment discharge: Impact from natural and anthropogenic changes. Sci. Rep.-UK 5, 12581.

Yun, C., 2004. Recent evolution of Yangtze Estuary and its mechanisms. China Ocean Press, Beijing, China (in Chinese).

Zhou, Z., Coco, G., Townend, I., Olabarrieta, M., van der Wegen, M., Gong, Z., D Alpaos, A., Gao, S., Jaffe, B.E., Gelfenbaum, G., He, Q., Wang, Y., Lanzoni, S., Wang, Z., Winterwerp, H., Zhang, C., 2017. Is “Morphodynamic Equilibrium” an oxymoron? Earth-Sci. Rev. 165, 257-267.

Zhu, L., He, Q., Shen, J., Wang, Y., 2016. The influence of human activities on morphodynamics and alteration of sediment source and sink in the Changjiang Estuary.

Geomorphology 273, 52-62.

Figure

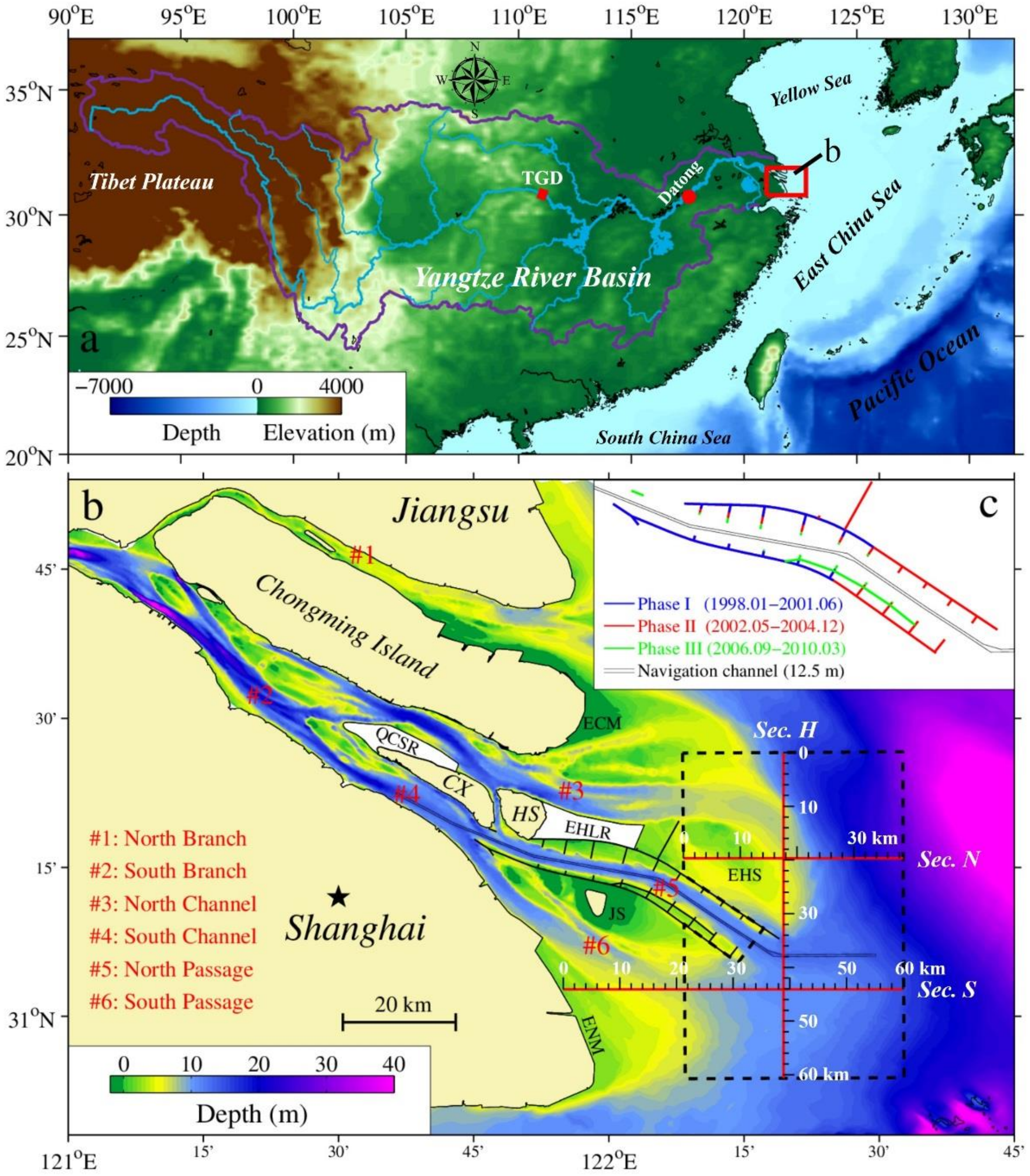

Fig. 1 (a) Map of the Yangtze River Basin and the location of the Yangtze Estuary (rectangle); (b) the Yangtze Estuary with bathymetry observed in 2010 referred to mean sea level (MSL); (c) the construction phases of the Deep Navigation Channel project. The dashed lines in (b) denote the boundary of the study area, and the ruler lines represent three sections (Sec. N, Sec. S and Sec. H). ECM: East Chongming mudflat; EHS: East Hengsha Shoal; JS: Jiuduansha Shoal; ENM: East Nanhui mudflat; CX: Changxing Island; HS: Hengsha Island; QCSR: Qingcaosha Reservoir; and EHLR: East Hengsha Land Reclamation.

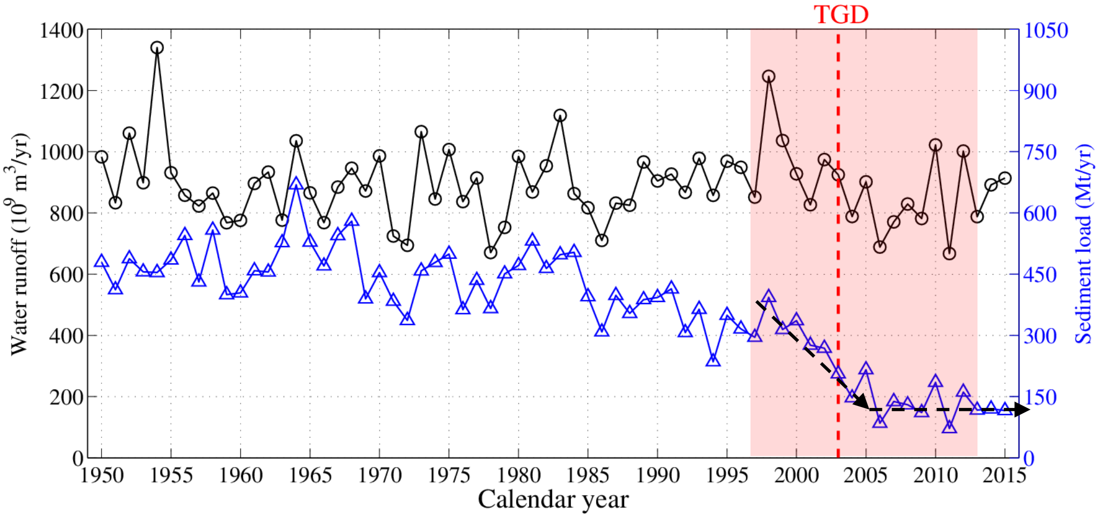

Fig. 2 Annual river runoff (circles) and suspended sediment load (triangles) since 1950 measured at Datong station. The vertical dash line represents the closure of the Three Gorge Dam (TGD) in 2003. The shading area represents the study period 1997-2013.

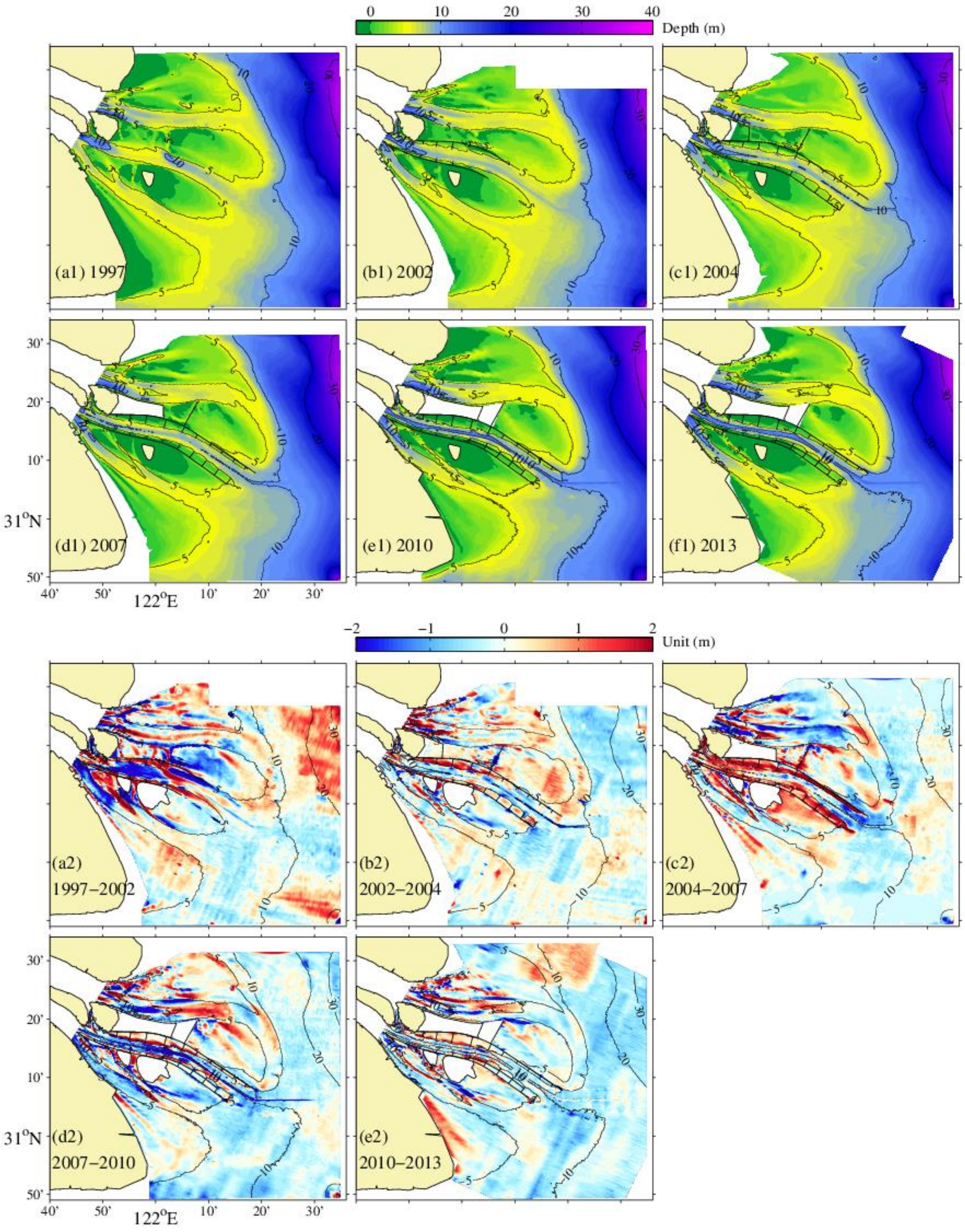

Fig. 3 Bathymetry (a1-f1) and erosion/deposition patterns (a2-e2) of the Yangtze mouth bar area and adjacent subaqueous delta from 1997 to 2013. The isobaths in the latter year are presented in a2-e2. The water depth and isobaths refer to the theoretical, lowest tidal datum.

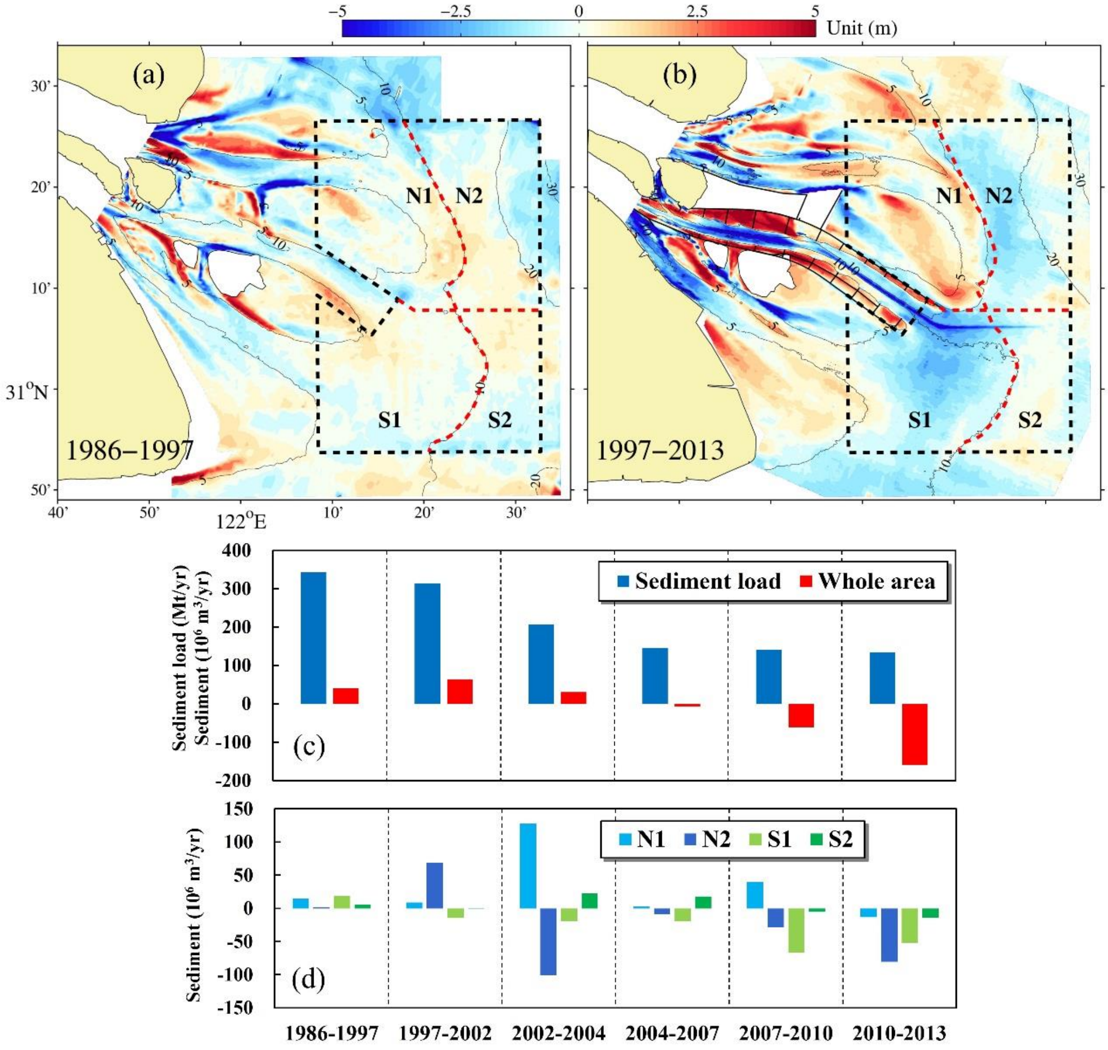

Fig. 4 (a) Erosion/deposition pattern of the mouth bar area in 1986-1997; (b) Erosion/deposition pattern of the mouth bar area in 1997-2013; (c) Annual-mean sediment load at Datong station and yearly net volume changes of the whole study area and (d) yearly net volume changes of four sub-areas as shown in (a) and (b). The dredged navigation channel is excluded in sediment volume calculations. The red dashed line separating the Area N1 and N2 (also the Area S1 and S2) in (a) and (b) is the 10 m isobath in 1997. The contours in (a) and (b) denote the isobaths in 1997 and 2013, respectively, referring to the theoretical, lowest tidal datum.

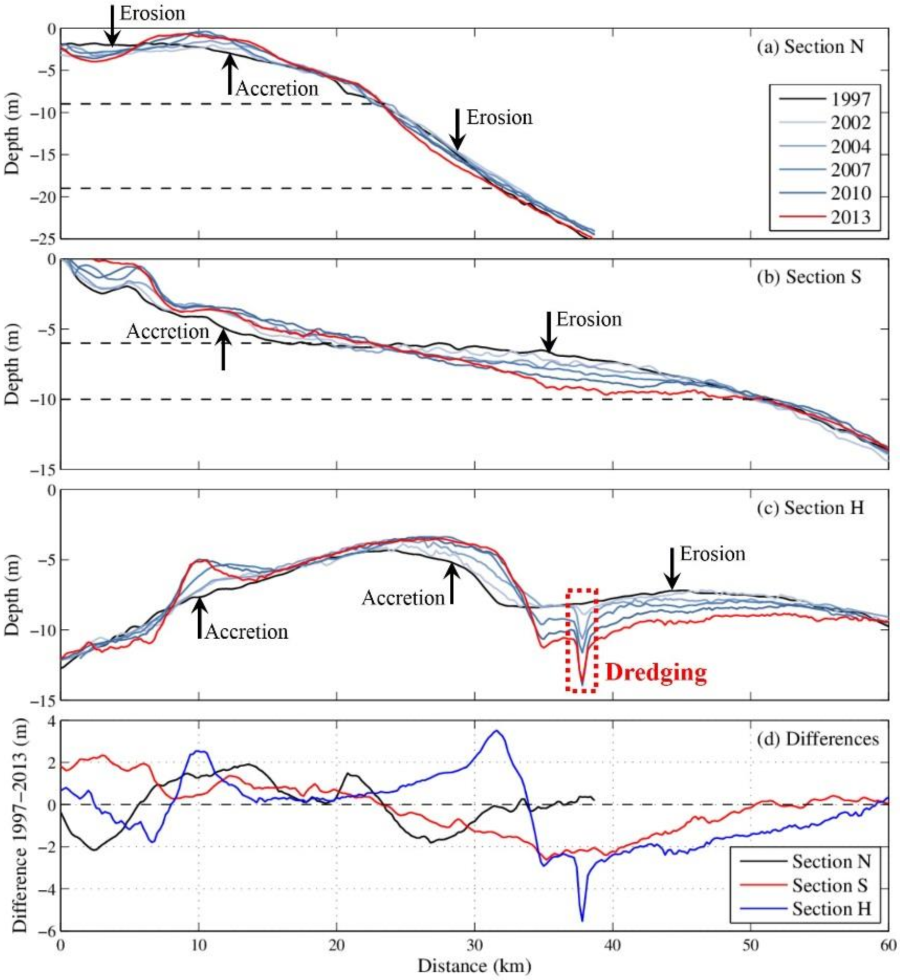

Fig. 5 Variations of three typical sections from 1997 to 2013 (a, b, c) (heading seaward for the Section N and S and southward for the Section H, see Fig. 1b for the locations) and the differences of the sections between 1997 and 2013 (d) (the water depth refers to the theoretical, lowest tidal datum; positive represents accretion and negative represents erosion).

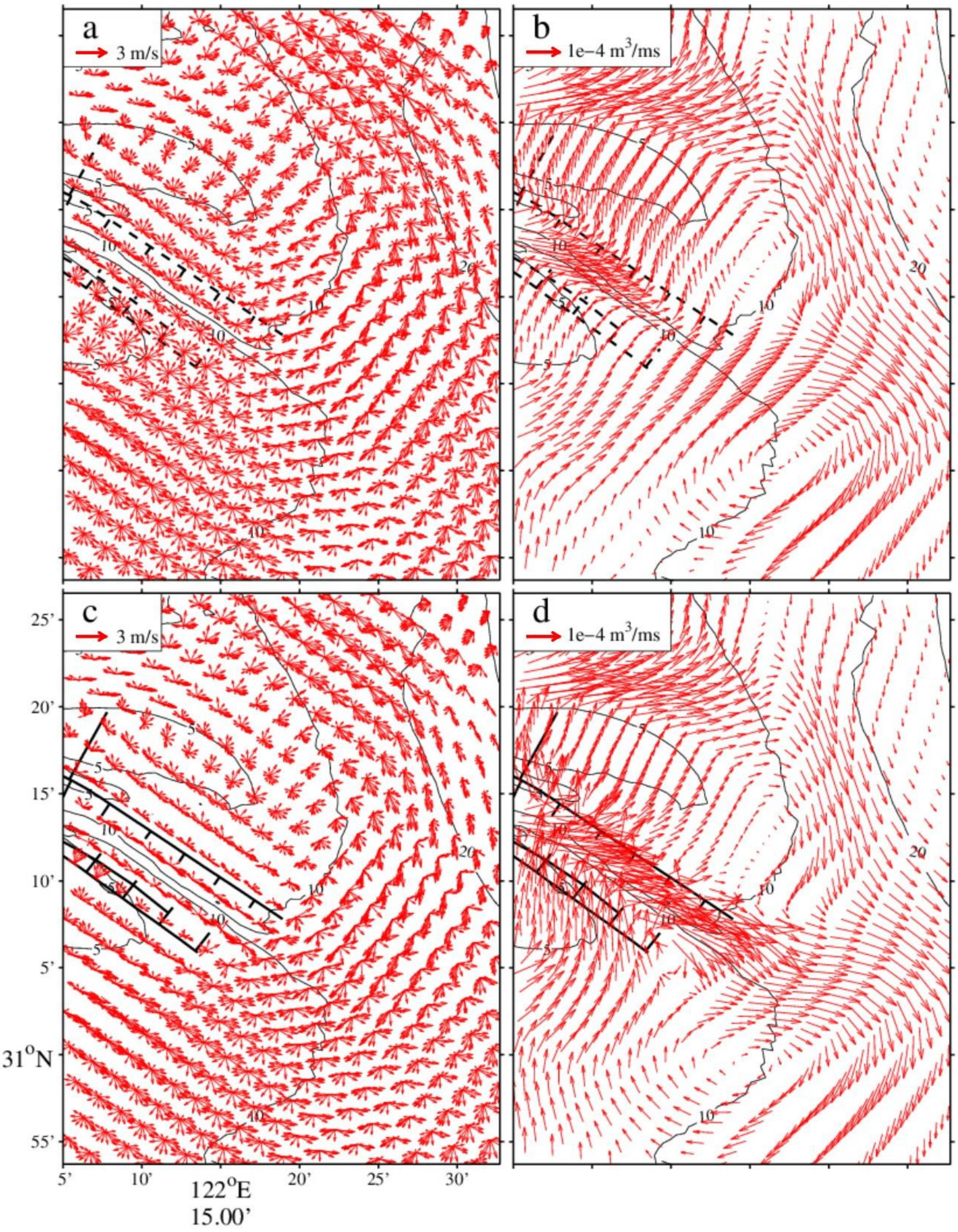

Fig. 6 Feathers of currents during spring tide (a, c) and monthly-averaged sediment flux (b, d) without (a, b) and with (b, d) training walls. Contours denote the isobaths in 2002 referred to MSL.

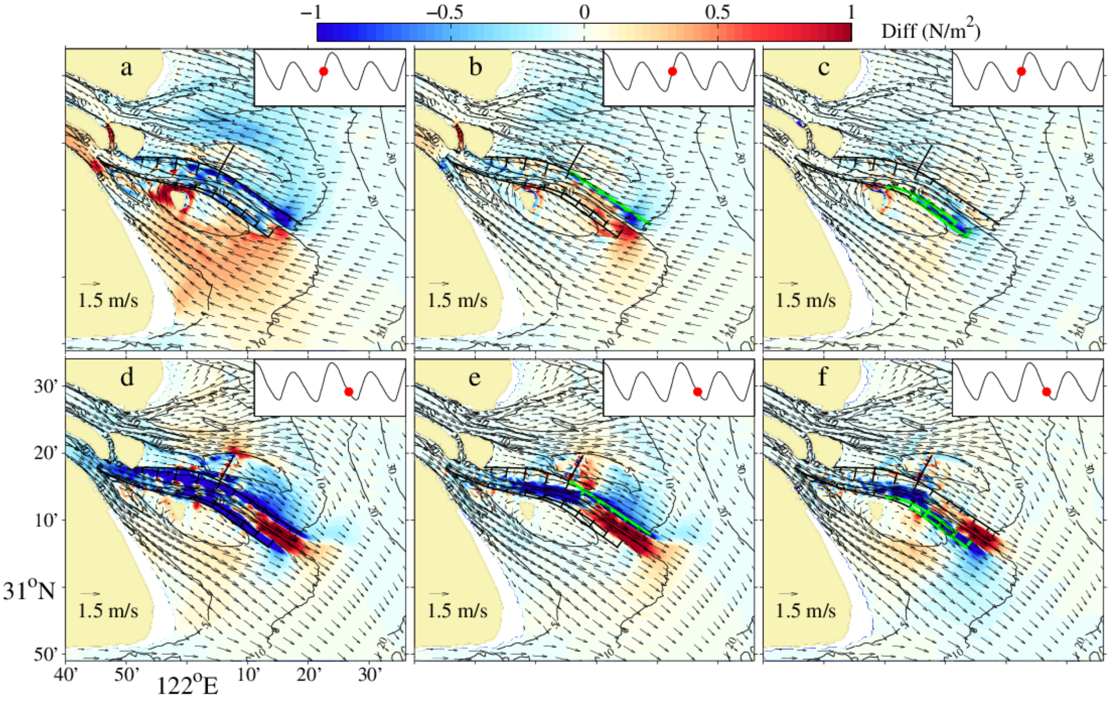

Fig. 7 Tidal currents (arrows) and differences of bed shear stress (background color) between model runs with and without all training walls (a, d), the eastern half of the northern training walls (b, e) and the eastern half of the southern training walls (c, f) (in green color) at flood maximum (a, b, c) and ebb maximum (d, e, f). Contours denote the isobaths in 2002 referred to MSL.

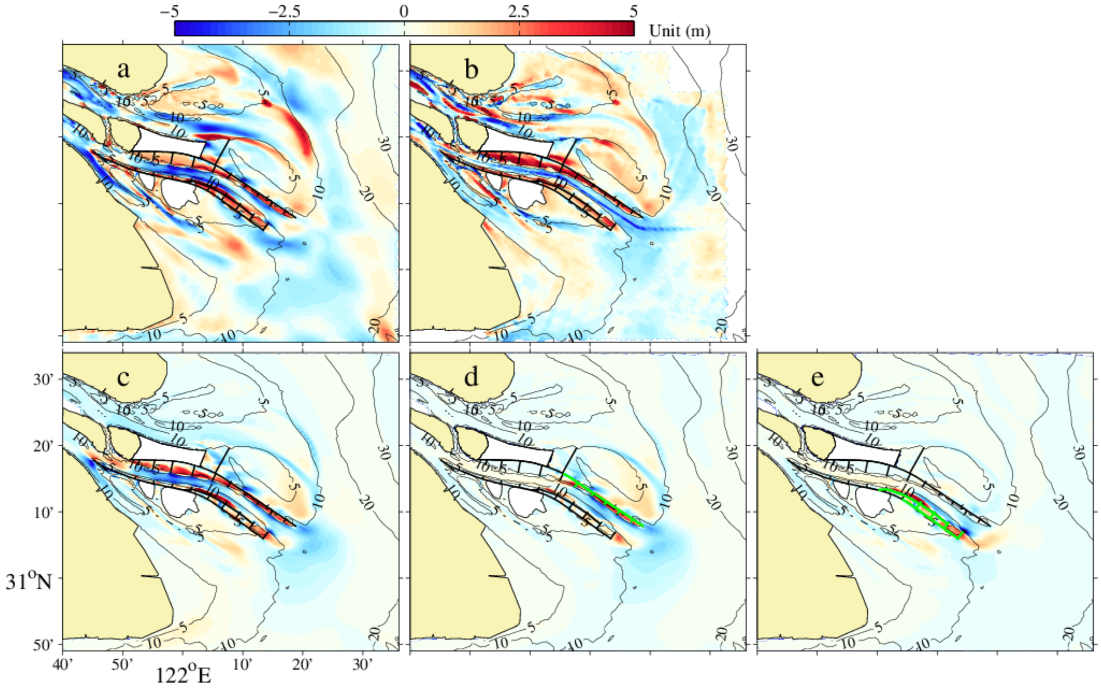

Fig. 8 Modeled (a) and observed (b) erosion/deposition patterns in 2002-2010, and the differences between model runs with and without all training walls (c), the eastern half of the northern training walls (d) and the eastern half of the southern training walls (e) (in green color). Contours denote the isobaths in 2010 referred to MSL.

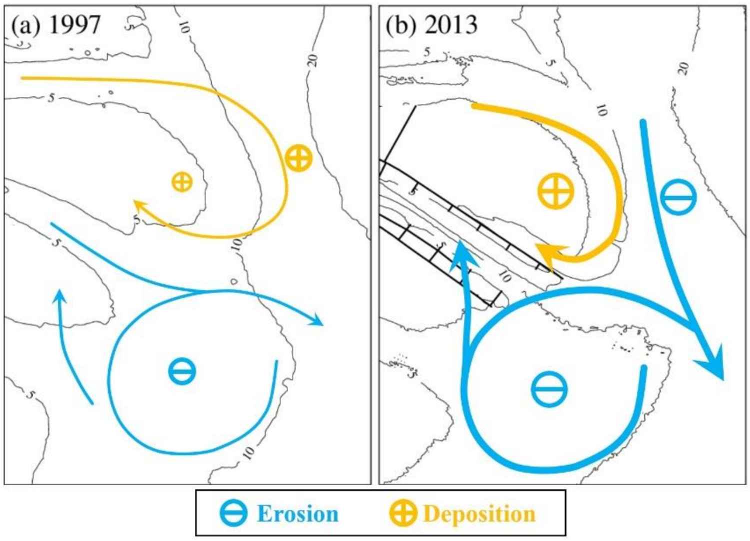

Fig. 9 Schematized maps of sediment transport paths (arrows) and specific erosion/deposition locations within the study area in 1997 (a) and 2013 (b)

Supplementary information for:

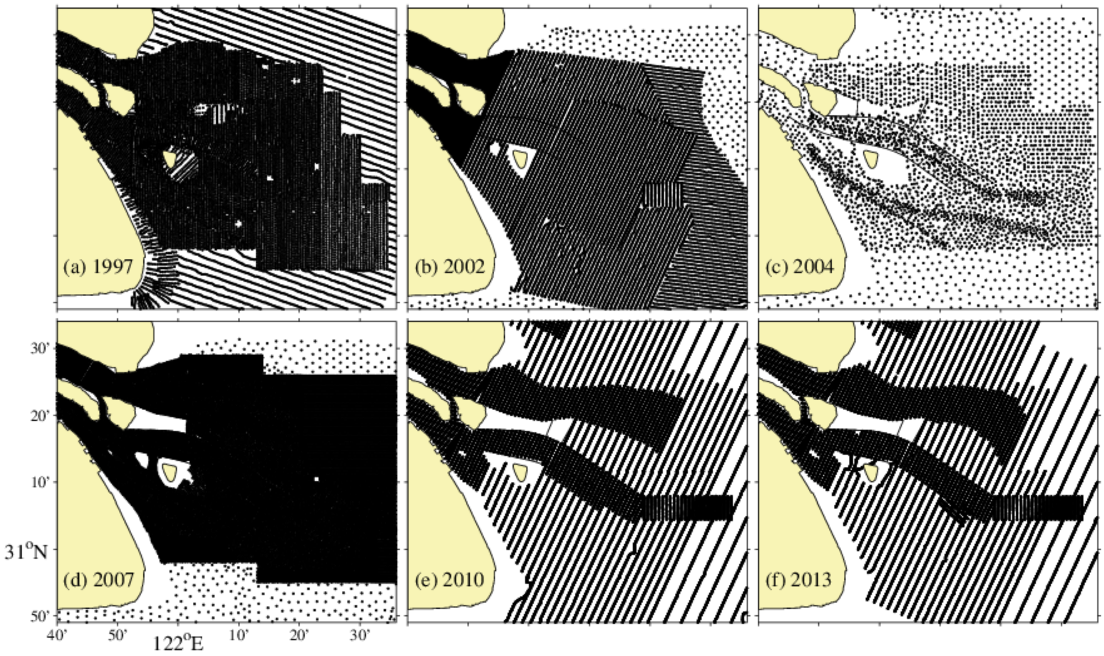

Fig. S1 Bathymetric sample points observed in different years used in this study.

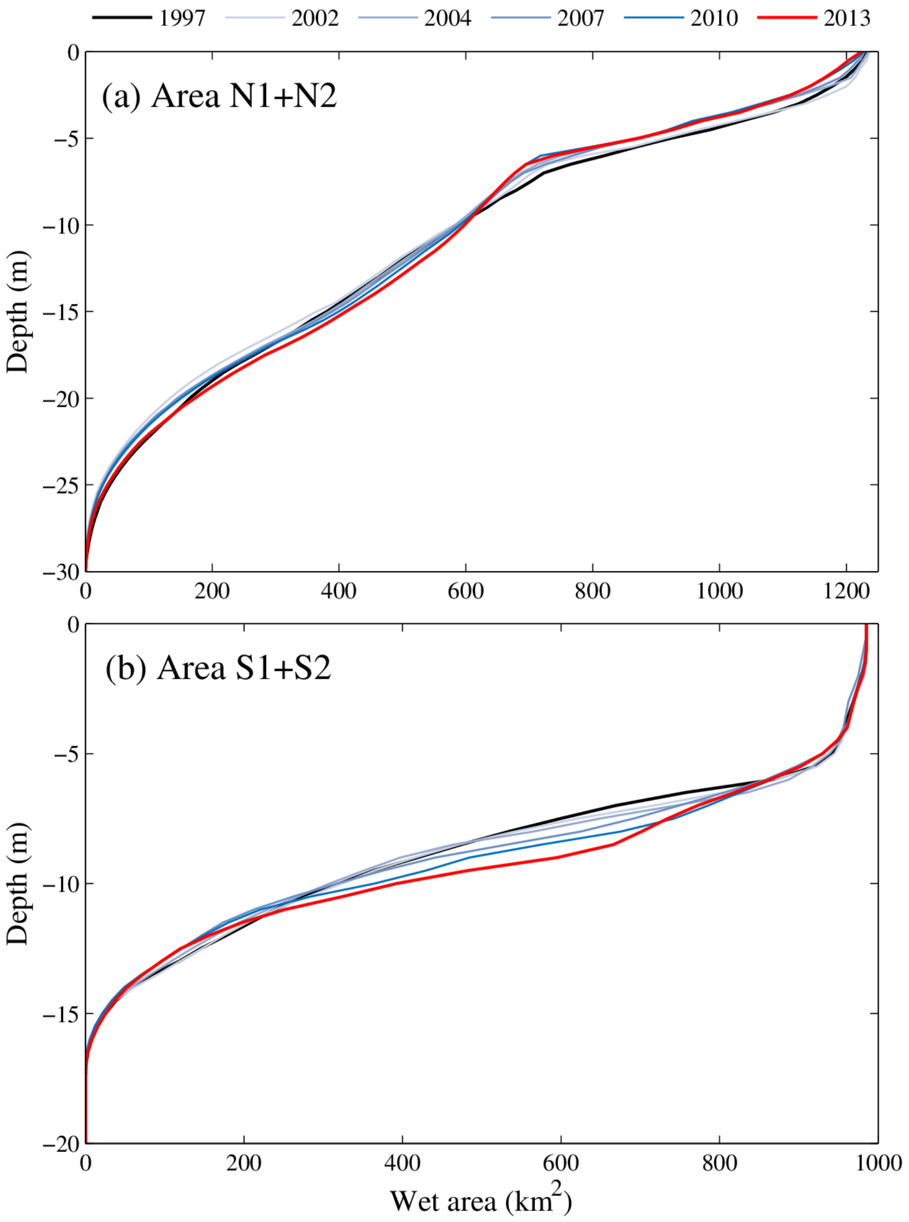

Fig. S2 Hypsometry curves of the northern part (a) and south part (b) from 1997 to 2013. See Fig. 4a for the domains of the areas.

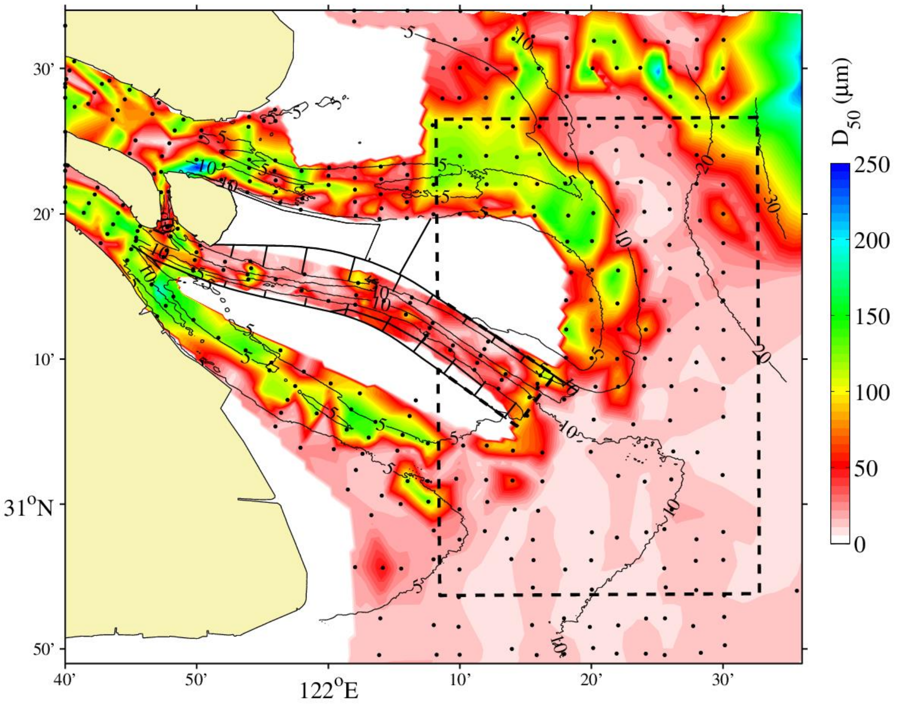

Fig. S3 Median grain size (D_{50}) at the mouth bar area (black dots denote bed surface sediment samples in September 2015, and dashed line denotes the boundary of the study area as shown in Fig. 1b).

Tab. S1 Collected bathymetry maps and navigational charts used in this study.

Year	Map Title	Scale	Sources	Survey	Publish
1997	Changjiang Estuary and adjacent area	1:50,000	Yangtze Estuary Waterway Administration Bureau, Ministry of Transport, PRC (YEWAB)	1997	
2002	Changjiang Estuary and adjacent area	1:50,000	YEWAB	2002.12	
	Southern part of Changjiang Estuary	1:130,000	Navigation Guarantee Department of the Chinese Navy Headquarters (NGDCNH)	2001~2002	2002.12
2004	Changjiang Estuary and adjacent area	1:120,000	Maritime Safety Administration, PRC	2004	2004.12
	Jigujiao to Hengsha Island	1:75,000		2004	2005.09
2007	Changjiang Estuary and adjacent area	1:50,000	YEWAB	2007.08	
	Southern part of Changjiang Estuary	1:130,000	NGDCNH	2007~2008	2009.04
2010	Changjiang Estuary and adjacent area	1:50,000	YEWAB	2010.08	
2013	Changjiang Estuary and adjacent area	1:50,000	YEWAB	2013.08	

Tab. S2 Statistics of the erosion/deposition area and volume and net accretion rate in the whole area and the annual-mean sediment load at Datong Station (Note that the dredged navigation channel is excluded. See Fig. 4a for the domain of the study area. Positive values represent accretion, and negative values represent erosion).

			1986-1997	1997-2002	2002-2004	2004-2007	2007-2010	2010-2013
Sediment load		(Mt yr^{-1})	**343**	**314**	**207**	**146**	**141**	**134**
Erosion and accretion over the whole study area	Area	(km^2)	2223	2223	2223	2223	2223	2223
	Erosion	Area (%)	33	42	48	54	64	72
		Volume (10^6 m^3 yr^{-1})	−30.0	−65.5	−188.5	−134.4	−153.3	−204.2
	Accretion	Area (%)	67	58	52	46	36	28
		Volume (10^6 m^3 yr^{-1})	70.6	129.1	219.2	127.4	92.6	44.5
	Net	Volume (10^6 m^3 yr^{-1})	**40.6**	**63.6**	**30.7**	**−7.0**	**−60.7**	**−159.6**
		Rate (mm yr^{-1})	18.2	28.6	13.8	−3.2	−27.3	−71.8

Tab. S3 Statistics of the erosion/deposition area and volume and net accretion rate in the four sub-areas (Note that the dredged navigation channel is excluded. See Fig. 4a for the domains of the sub-areas. Positive values represent accretion, and negative values represent erosion).

			1986-1997	1997-2002	2002-2004	2004-2007	2007-2010	2010-2013
Area N1	Total area	(km^2)	654	654	654	654	654	654
	Erosion	Area (%)	32	39	15	52	39	58
		Volume (10^6 m^3 yr^{-1})	−10.1	−30.2	−9.6	−55.2	−30.4	−37.5
	Accretion	Area (%)	68	61	85	48	61	42
		Volume (10^6 m^3 yr^{-1})	24.7	39.2	137.3	57.9	70.3	24.4
	Net	Volume (10^6 m^3 yr^{-1})	**14.6**	**9.0**	**127.7**	**2.7**	**39.8**	**−13.2**
		Rate (mm yr^{-1})	22.3	13.7	195.2	4.1	60.9	−20.1
Area N2	Total area	(km^2)	584	584	584	584	584	584
	Erosion	Area (%)	44	8	86	57	76	91
		Volume (10^6 m^3 yr^{-1})	−14.3	−2.0	−108.1	−29.2	−36.0	−84.1
	Accretion	Area (%)	56	92	14	43	24	9
		Volume (10^6 m^3 yr^{-1})	16.0	70.6	7.4	20.6	7.2	3.6
	Net	Volume (10^6 m^3 yr^{-1})	**1.8**	**68.6**	**−100.7**	**−8.6**	**−28.8**	**−80.6**
		Rate (mm yr^{-1})	3.0	117.4	−172.5	−14.8	−49.3	−138.0
Area S1	Total area	(km^2)	664	664	664	664	664	664
	Erosion	Area (%)	20	66	53	64	81	69
		Volume (10^6 m^3 yr^{-1})	−2.0	−22.8	−58.7	−46.6	−73.6	−65.8
	Accretion	Area (%)	80	34	47	36	19	31
		Volume (10^6 m^3 yr^{-1})	20.7	8.3	39.8	27.6	7.0	14.0
	Net	Volume (10^6 m^3 yr^{-1})	**18.7**	**−14.5**	**−19.0**	**−19.0**	**−66.6**	**−51.8**
		Rate (mm yr^{-1})	28.1	−21.8	−28.5	−28.6	−100.3	−78.0
Area S2	Total area	(km^2)	321	321	321	321	321	321
	Erosion	Area (%)	41	58	34	29	59	73
		Volume (10^6 m^3 yr^{-1})	−3.7	−10.5	−12.1	−3.4	−13.2	−16.7
	Accretion	Area (%)	59	42	66	71	41	27
		Volume (10^6 m^3 yr^{-1})	9.3	11.0	34.7	21.4	8.1	2.7
	Net	Volume (10^6 m^3 yr^{-1})	**5.5**	**0.5**	**22.6**	**18.0**	**−5.1**	**−14.1**
		Rate (mm yr^{-1})	17.3	1.6	70.4	56.0	−16.0	−43.8